

# Digital Quantum Key Distribution with Continuous-Mode Formalism

Ziyang Chen,<sup>1</sup> Xiangyu Wang,<sup>2</sup> Zhengyu Li,<sup>3</sup> Song Yu,<sup>2</sup> and Hong Guo<sup>1,\*</sup>

<sup>1</sup>*State Key Laboratory of Advanced Optical Communication Systems and Networks, School of Electronics, and Center for Quantum Information Technology, Peking University, Beijing 100871, China*

<sup>2</sup>*State Key Laboratory of Information Photonics and Optical Communications, Beijing University of Posts and Telecommunications, Beijing 100876, China*

<sup>3</sup>*Huawei Technologies Co., Ltd., Shenzhen 518129, China*

(Dated: June 2022)

Quantum key distribution (QKD) provides an attractive key-sharing technology for remote users with information-theoretic security. QKD with continuous variables offers extraordinary superiority by the use of standard telecom components, thereby moving toward large-scale metropolitan applications. However, from lab demonstrations to in-field realizations, the primary task is to deal with gaps between practical systems and theoretical models. Herein, we present a continuous-mode formalism to close the loophole of fundamental single-mode assumption; this form exhibits a rigorous mapping between theoretical model and practical digital experiments by using temporal modes theory, which opens a new perspective of investigating the digital signal processing through a practical security model. The proposed practicality-oriented security analysis method paves the way to build cost-effective and classical compatible quantum networks by using non-ideal devices.

Quantum key distribution (QKD) [1–3] is a promising approach in the quantum information field, enabling distant peers to securely generate identical keys based on the laws of quantum physics, regardless of how powerful a potential attack is. The past three decades have witnessed rapid growth and development in the QKD domain [2], and QKD infrastructures deployed in the real world have provided security services for various applications [4–11], including point-to-point and network scenarios. Within the QKD family, continuous-variable QKD (CV-QKD) benefits from the use of off-the-shelf commercial telecom components [12–14] and provides a new pathway for cost-effective deployments in metropolitan networks.

During all 20 years since the pioneering CV-QKD protocol, namely the GG02 protocol [15], was proposed, the theory [16–22] and experimentation [23–28] of CV-QKD have experienced revolutionary progress. Remarkably, the theoretical security of the coherent-state protocol has been basically proved [19, 20]. This makes it possible for users to employ standard telecom components for secure key distribution; the tremendous breakthrough in experimentation even makes CV techniques competitive in real-world infrastructure developments [27, 29–31].

Although CV-QKD has achieved great success in theoretical and experimental settings, while moving forward from the theoretical to the practical security, significant interest in using theoretical tools to narrow the gap between the model’s assumption and true experiment still exists. For example, the newly developed discrete modulation technique is of great benefit in answering the doubt surrounding non-Gaussian modulation, and meanwhile provides technical potential beyond expectations [32, 33]. However, another theoretical argument for a fundamental assumption, namely single-mode quantum states, is rarely met in practice.

The security framework of CV-QKD is based on the quadrature-component measurement of one single mode. Unfortunately, the traditional single-mode assumption squashes the dimension of systems and this constraint poses severe limitations on practical analyses of security and performance. Practical systems often contain more abundant time- and frequency-domain characteristics than ideal single-mode cases: the transmitter (Alice) generates pulsed or continuous-wave (CW) coherent state with time-dependent forms, and the practical receiver (Bob) performs a series of non-ideal operation, including band-limited detection, analog-to-digital converter (ADC) sampling, and digital processing. This makes it sophisticated to well define the measured quadratures in practical continuous-mode cases.

In this Letter, toward next generation digital CV-QKD systems, we focus on a generalized practical system model and establish a CV-QKD framework with a continuous-mode formalism. Our analysis, for the first time to the best of our knowledge, indicates that CV-QKD can still maintain its security under a continuous-mode assumption, which is an indispensable step towards practical applications. More specifically, by introducing technologies from continuous-mode quantum optics, the receiver’s quadrature and the shot noise unite (SNU) under digital discrete-time sampling can be redefined by exploiting *temporal modes theory* [3, 35, 36]. Treating the whole receiver as one new temporal mode (TM), which is determined by the envelope of the local oscillator (LO), impulse response function (IRF), ADC’s sampling time, and digital operation, the actual measurement result is the projection of this TM on the measured states.

Based on our work, state-of-the-art classical communication toolboxes, such as pulse multiplexing, clock synchronization, dispersion compensation, and digital signal processing (DSP) technologies, are expected to be directly employed in the analysis of CV-QKD, which il-

\* E-mail: hongguo@pku.edu.cn

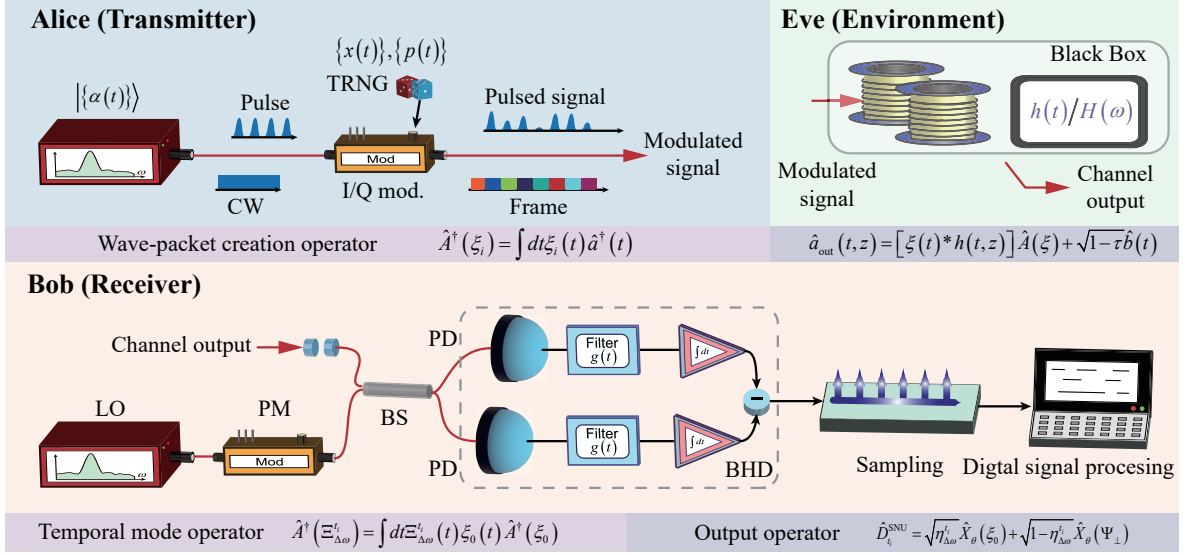


FIG. 1. Structure of continuous-mode digital CV-QKD protocol. Alice prepares a continuous-mode coherent state  $|\{\alpha(t)\}\rangle$  as the carrier, the quadratures of which are modulated by Gaussian distributed random numbers. The carrier can be either a continuous wave or pulsed coherent state with arbitrary form of envelope  $\{\xi_i(t)\}$ . Then, the encoded states are transmitted through the time-dependent quantum channel, which is controlled by Eve. Afterward, the received signal interferes with the local oscillator (LO) at Bob's side by a balanced homodyne detector (BHD), placed after a balanced beam splitter. The LO can be generated at either Alice's or Bob's side, and phase modulations on the LO are performed to measure quadratures randomly. The BHD is modeled by the subtraction between two practical photodetectors with limited bandwidth and integration effect. The discrete-time outcomes are obtained by sampling devices, and then the final keys are extracted by a digital signal processing (DSP) procedure. A detailed description is provided in the Supplemental Material. TRNG, true random number generator; CW, continuous wave; PM, phase modulation; BS, beam splitter; PD: photodetector.

illustrates the importance of our work. Remarkably, the evolution of pulse propagation and selection of sampling position on pulses have significant impacts on the key rate, which could not be analyzed in previous studies. These results are crucial for high-rate secure key distribution.

*Temporal modes of continuous-mode states.*—We now illustrate the state preparation in a more general situation; that is, the case of non-single-mode quantum states.

Recall that traditional CV-QKD assumes that the quantum state is represented by the creation and annihilation operators in terms of discrete cases (given by  $\hat{a}_i^\dagger, \hat{a}_i$ ) of the ideal single-mode electrical field. In practical experiments, however, the time-domain and spectrum characteristics of quantum states are crucial, especially when considering practical devices. Therefore, more generally, we extend the electrical field to the continuous-mode form by performing transformation of the annihilation operator  $\hat{a}_i \rightarrow (\Delta\omega)^{\frac{1}{2}} \hat{a}(\omega)$ , where  $\Delta\omega$  denotes the mode spacing and  $\hat{a}(\omega)$  is the continuous-mode operator, which satisfies the commutation relation  $[\hat{a}(\omega), \hat{a}^\dagger(\omega')] = \delta(\omega - \omega')$ . This technique is widely used in studying continuous-mode quantum optics [3].

In time-evolution scenarios [38], especially when the measured signals are pulses, it is always useful to define the Fourier transforms of continuous-mode field operators in the time domain, namely  $\hat{a}(t)$ , to analyze the

behavior of time-dependent quantum states. It is difficult to analyze the behavior of continuous-mode operators directly. Therefore, to analyze the system at different signal-generated times, we use the infinitely countable complete orthonormal set of functions  $\{\xi_i(t)\}_{i=1}^\infty$  as non-continuous basis functions to expand the operator  $\hat{a}(t)$ , where  $\xi_i(t)$  is also the envelope of the  $i$ th wave packet. The expansion of the continuous-mode operator is given by  $\hat{a}(t) = \sum_i \xi_i(t) \hat{A}(\xi_i)$ , and in quantum field theory, the photon wave-packet creation operator  $\hat{A}^\dagger(\xi_i)$  is defined as [2–4]

$$\hat{A}^\dagger(\xi_i) = \int dt \xi_i(t) \hat{a}^\dagger(t), \quad (1)$$

which means that a quantum state with an envelope  $\xi_i(t)$  is generated at position  $t$ , also known as the TM [35, 36]. The TM operator also obeys the commutation relation, which reads

$$[\hat{A}(\xi_i), \hat{A}^\dagger(\xi_j)] = \delta_{ij}. \quad (2)$$

It is then important to define the continuous-mode coherent state  $|\{\alpha(t)\}\rangle$  as the tensor product of wave-packet coherent states  $|\gamma_i\rangle$ , given by [3]

$$|\{\alpha(t)\}\rangle = \prod_i \hat{D}(\gamma_i) |0\rangle = |\{\gamma_i\}\rangle, \quad (3)$$

where  $\gamma_i$  denotes the eigenvalue of a single wave-packet coherent state,  $|\gamma_i|^2$  represents the average photon number contained in one wave packet, and  $\hat{D}(\gamma_i) = \exp(\gamma_i \hat{A}^\dagger(\xi_i) - \gamma_i^* \hat{A}(\xi_i))$  is the displacement operator. The wave-packet coherent state has all the usual properties of Glauber coherent states, and obeys the eigenvalue equation:

$$\hat{A}(\xi_i) |\gamma_i\rangle = \gamma_i |\gamma_i\rangle. \quad (4)$$

Under this notation, the quadrature operator of wave-packet coherent states for phase angle  $\theta$  can be defined, which is given as

$$\hat{X}_\theta(\xi_i) = \hat{A}^\dagger(\xi_i) \exp(i\theta) + \hat{A}(\xi_i) \exp(-i\theta). \quad (5)$$

The understanding of Eq. (5) is the core of the whole continuous-mode analysis. For traditional CV-QKD, the measured quadrature operator reflects the quadrature information of a single-mode quantum state, while for continuous-mode CV-QKD, the measured quadrature operator is used to define the quadrature of a TM (or a wave-packet). Alice's modulation of a quantum state with arbitrary form can be mapped to the preparation of a TM. Consequently, if the quadrature component of the TM can be measured and used for generating keys, the security analysis of single-mode CV-QKD can be continued to use, resulting from the same form of the commutation relation (shown in Eq. (2)) with that of the single-mode case.

*Measurement and sampling.*—The scenario becomes more involved after considering the band-limited homodyne detection and sampling process (see the Supplemental Material for detailed derivation).

Here, for the rigorous security analysis of CV-QKD, we focus on the measurement results of a practical detection model with arbitrary IRF, namely,  $g(t)$ , which reads

$$\hat{O}(t) = \int_t^{t+T} dt' [\hat{a}^\dagger(t') \hat{a}_{\text{LO}}(t') + \hat{a}_{\text{LO}}^\dagger(t') \hat{a}(t')] * g(t), \quad (6)$$

where  $T$  denotes the integration time of the photodetector (PD). Assume that the LO is a classical field, given by  $\alpha_{\text{LO}}(t) = \mu_{\text{LO}}^{1/2} \xi_{\text{LO}}(t) \exp(i\omega_{\text{LO}}t + i\theta)$ , where  $\mu_{\text{LO}}$  denotes the average number of photons contained in each LO pulse, and  $\xi_{\text{LO}}(t)$  is the envelope of the LO. Through the band-limited measurement operator given by Eq. (6) and the sampling model, the output photocurrent operator  $\hat{D}_{t_i}$  at sampling time  $t_i$  can be then obtained by

$$\hat{D}_{t_i} = \frac{T}{\Delta t_s} \mu_{\text{LO}}^{1/2} \int dt \xi_{\text{LO}}(t) G^{t_i, \Delta t_s}(t) \hat{X}_a^{\omega_{\text{LO}}t + \theta}(t), \quad (7)$$

where  $\Delta t_s$  denotes the sampling-hold time;  $G^{t_i, \Delta t_s}(t') = \int_{t_i}^{t_i + \Delta t_s} dt g(t - t')$  is the integrated detection function related to detector's IRF;  $\hat{X}_a^{\omega_{\text{LO}}t + \theta}(t)$  denotes the quadrature operator of the input state  $\hat{a}(t)$  under the LO with

central frequency  $\omega_{\text{LO}}$  and phase  $\theta$ , which is given by

$$\hat{X}_a^{\omega_{\text{LO}}t + \theta}(t) = \exp[i(\omega_{\text{LO}}t + \theta)] \hat{a}^\dagger(t) + \exp[-i(\omega_{\text{LO}}t + \theta)] \hat{a}(t). \quad (8)$$

Using Eq. (7), we can acquire the sampling results of the continuous-mode state  $\hat{a}(t)$  at any time  $t_i$ . Assuming the sampling interval is  $T_s$ , the period of the transmitted signal is  $T_r$ , we can obtain  $N$  sampling points  $\{\hat{D}_{t_i}\}_{i=1}^N$  in one period, where  $N = T_r/T_s$  and  $t_i = iT_s$ . The measurement results in a period can be simply expressed by a single sampling point, or can be obtained by weighted averaging of multi-points. In the following part, we analyze the situation of using one point as the measurement result in one period, and the statistical information is obtained from the measurement points of several periods. The same method can be used to analyze the multi-point weighted average cases.

*SNU calibration and normalization.*—In order to normalize the measured data, one key step is to define and calibrate the SNU, which is the most distinguish phase from classical optical communication. By defining the variance of shot noise at sampling time  $t_i$  as  $\sigma_{\text{SNU}}^2(t_i) = \langle 0 | \hat{D}_{t_i} \hat{D}_{t_i} | 0 \rangle$ , the standard deviation of the shot noise is obtained, given by

$$\sigma_{\text{SNU}}(t_i) = \frac{T}{\Delta t_s} \mu_{\text{LO}}^{1/2} \int dt \xi_{\text{LO}}(t) G^{t_i, \Delta t_s}(t). \quad (9)$$

where the statistical data comes from the measurement results of different periods at time label  $t_i$ .

After the SNU normalization, the measured data is obtained by dividing the sampled photocurrent operator by the standard deviation of the shot noise, namely,  $D_{t_i}^{\text{SNU}} = \frac{\hat{D}_{t_i}}{\sigma_{\text{SNU}}(t_i)}$ , which is given by

$$\hat{D}_{t_i}^{\text{SNU}} = \int dt \frac{\xi_{\text{LO}}(t) G^{t_i, \Delta t_s}(t)}{\sigma_{\text{SNU}}(t_i)} \hat{X}_a^{\omega_{\text{LO}}t + \theta}(t). \quad (10)$$

It is crucial to construct the whole receiver as a new TM, namely,  $\Xi_{\omega_{\text{LO}}}^{t_i}(t)$ , given by

$$\Xi_{\omega_{\text{LO}}}^{t_i}(t) = \frac{\xi_{\text{LO}}(t) G^{t_i, \Delta t_s}(t)}{\sigma_{\text{SNU}}(t_i)} \exp(i\omega_{\text{LO}}t), \quad (11)$$

and it is not difficult to prove that this mode meets the normalization condition  $\int dt |\Xi_{\omega_{\text{LO}}}^{t_i}(t)|^2 = 1$ . This TM represents a basis function in the phase space rotating at speed  $\omega_{\text{LO}}$ , which is related to the sampling point  $t_i$  and all measurement devices.

Based on the TM as described in Eq. (11), using similar form of Eq. (1), we can also define a TM creation operator as

$$\hat{A}^\dagger(\Xi_{\omega_{\text{LO}}}^{t_i}) = \int dt \Xi_{\omega_{\text{LO}}}^{t_i}(t) \hat{a}^\dagger(t), \quad (12)$$

which can be treated as the projection of operator  $\hat{a}^\dagger(t)$  on the basis  $\Xi_{\omega_{\text{LO}}}^{t_i}(t)$ . Consequently, the simplified result of Eq. (10) in terms of TMs is then rewritten as

$$\begin{aligned}\hat{D}_{t_i}^{\text{SNU}} &= \hat{A}^\dagger(\Xi_{\omega_{\text{LO}}}^{t_i}) \exp(i\theta) + \hat{A}(\Xi_{\omega_{\text{LO}}}^{t_i}) \exp(-i\theta) \\ &= \hat{X}_\theta(\Xi_{\omega_{\text{LO}}}^{t_i}).\end{aligned}\quad (13)$$

Therefore, all the measurement results can be treated as the quadrature measurement of the TM  $\Xi_{\omega_{\text{LO}}}^{t_i}$ , which is composed of the parameters from both measurement devices and the signal to be measured.

In the TM description, we can see that SNU calibration is actually the process of calibrating measurement devices. All the spectrum-related information of detector and LO are involved. This explains why SNU calibration is so important in CV-QKD. If the calibration of the measurement device is incorrect, it will cause the deviation of the projection of the detection mode on the measured state.

*Projection on measured quantum states.*—The whole measurement process under the TM representation is equivalent to the projection of the receiver's TM to the TM of the measured state, and vice versa. Therefore, the next step is to know the deviation of the measurement results from the real measured states.

Now considering a practical situation where the measured state is an arbitrary wave-packet coherent state  $|\gamma_s\rangle$  with the eigenvalue equation given by Eq. (4), we can expand operator  $\hat{a}(t) = \xi_0(t) \exp(i\omega_s t) \hat{A}(\xi_0)$ , and Eq. (98) is rewritten as (where  $\omega_s$  is the central frequency of signals):

$$\hat{A}^\dagger(\Xi_{\Delta\omega}^{t_i}) = \int dt \Xi_{\Delta\omega}^{t_i}(t) \xi_0(t) \hat{A}^\dagger(\xi_0), \quad (14)$$

where  $\int dt \Xi_{\Delta\omega}^{t_i}(t) \xi_0(t)$  quantifies the overlapping envelope (or basis) between measured signals and the receiver, under the phase space rotating at speed  $\Delta\omega = \omega_s - \omega_{\text{LO}}$ , and it is also treated as the projection of the TM  $\Xi_{\Delta\omega}^{t_i}(t)$  on the basis  $\xi_0(t)$ .

Using the Gram-Schmidt orthogonalization procedure, we can map the measured operator from the basis  $\Xi_{\Delta\omega}^{t_i}(t)$  to the set of bases  $\{\xi_0(t), \Psi_\perp(t)\}$ . In this transformation, the basis  $\Xi_{\Delta\omega}^{t_i}(t)$  represents the receiver's mode-matched basis function;  $\xi_0(t)$  is the projection of the receiver's basis onto the input states, and the orthogonal basis  $\Psi_\perp(t)$  is the projection of the measured results onto the non-mode-matched background. An interesting result of measurement outcome is obtained, which reads

$$\hat{D}_{t_i}^{\text{SNU}} = \sqrt{\eta_{\Delta\omega}^{t_i}} \hat{X}_\theta(\xi_0) + \sqrt{1 - \eta_{\Delta\omega}^{t_i}} \hat{X}_\theta(\Psi_\perp), \quad (15)$$

where

$$\sqrt{\eta_{\Delta\omega}^{t_i}} = \int dt \Xi_{\Delta\omega}^{t_i}(t) \xi_0(t) \quad (16)$$

is the overlapping basis between the measurement mode

and the input signal;  $\hat{X}_\theta(\xi_0)$  and  $\hat{X}_\theta(\Psi_\perp)$  are the mode-matched and non-mode-matched quadratures, respectively. The first- and second-order moments of the non-mode-matched part under the measurement of input states vanish.

Note that the practical measurement result is actually equivalent to the attenuation of the real quadrature component caused by a mode-matched beam splitter, and its attenuation coefficient  $\sqrt{\eta_{\Delta\omega}^{t_i}}$  denotes the projection of the receiver's mode on the input quantum state, which results from the mismatch between the measurement device and the measured states. If and only if the mode matching occurs, namely,  $\Xi_{\Delta\omega}^{t_i}(t) = \xi_0(t)$ , the measurement results can truly reflect the quadrature information of measured states.

Moreover, Eq. (105) holds when the SNU calibration point and the measurement point used for key generation are at the same sampling position of the pulse, and the extremality of Gaussian states still holds in that case. However, if the the SNU calibration point and the measurement point used for key generation are at different sampling positions of the pulse, we need to modify the analysis by continuous-mode entanglement-based (EB) model, which is equivalent to replacing  $\eta_{\Delta\omega}^{t_i}$  with  $\eta_{\Delta\omega}(t_i, t_j)$  representing the correlation between sampling points  $t_i$  and  $t_j$ ; this is also equivalent to constructing another sampling-related TM. This situation occurs in systems where timing jitter exists. See the Supplemental Material for the analysis of the sampling deviation.

So far, we have analyzed the security of continuous-mode CV-QKD by defining the SNU normalized TMs of the receiver. Classical operations, such as digital down conversion, digital filtering, can still maintain the security by constructing proper receiver's TMs, and the traditional single-mode toolbox can be exploited directly, while the spectrum of transmitter and receiver will affect the system's performance. It is also worth noting that the spectrum calibration of communicated parties and DSP operation are important to maximize the efficiency of receiving quantum signals, so that we can recover the quadrature components more realistically.

For instance, if the receiver uses a filter with a spectrum similar to that of the transmitter, the modulated quadrature information can be recovered by only sampling the peak point. If the LO is a CW while the transmitted signal has some envelope form, Bob can conduct multi-point sampling for weighted averaging, and the weight can be set to the envelope shape of the transmitter. However, if the channel dispersion is large, the envelope of the received signal changes dramatically, which has a significant impact on the high-speed pulsed system. In the following part, we give an example to analyze the performance of high-repetition-rate CV-QKD systems in continuous-mode scenarios.

*Continuous-mode channel transmission.*—In practical experiments, compared with single-mode scenarios, it is



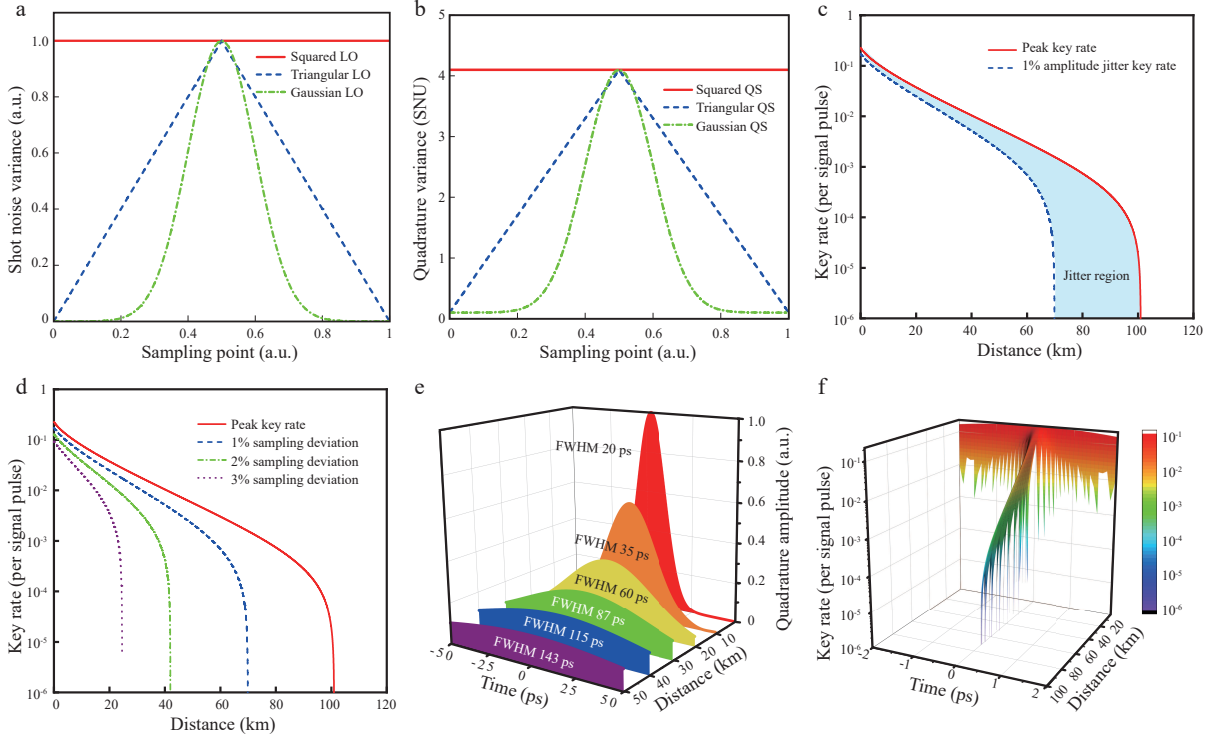


FIG. 2. Some simulation results of continuous-mode CV-QKD. **a.** Measured shot-noise variance at different sampling points. **b.** Measured quadrature variance at different sampling points. **c.** Secret key rates influenced by the timing jitter. **d.** Secret key rates influenced by sampling position. **e.** Evolution of Gaussian pulse with a full width at half-maximum of 20 ps in optical fibers, ignoring the fiber loss. **f.** Secret key rates of short-pulse propagation in fibers considering dispersion (the Gaussian-pulse as an example).

more common to consider quantum-state propagation with continuous-mode formalism. Through simplifications (see the Supplemental Material), the output mode after passing through the quantum channel can be obtained, given by [7, 42]

$$\hat{a}_{\text{out}}(t, z) = [\xi(t) * h(t, z)] \hat{A}(\xi) + \sqrt{1 - \tau} \hat{b}(t), \quad (17)$$

where  $h(t, z)$  is the channel transfer function in the time domain and  $\hat{b}(t)$  denotes the introduced averaged channel noise;  $A * B$  denotes the convolution between  $A$  and  $B$ . The Fourier transform of the channel transfer function can be easily obtained, expressed as

$$\mathcal{F}[h(t, z)] = \exp\left(-k_1 z + i k_1 \Omega z + i \frac{k_2}{2} \Omega^2 z\right), \quad (18)$$

where the second-order Taylor expansion of the real part of the wave vector is considered, and  $k_1$  and  $k_2$  denote the inverse group velocity and second-order dispersion coefficient, respectively. Equations (17) and (18) can well describe the evolution of continuous-mode states in the channel.

It is interesting to find that through the TM description, the new security analysis only increases the convolution effect of the channel transfer function on the signal envelope compared with traditional analysis, while other

forms of analysis are consistent. This result is useful for experiments, which reflects the similarity between CV-QKD and classical optical communication in the signal propagation process.

By calibrating the shapes of the signal and LO pulses before transmission, we can obtain every received pulse  $\xi_{\text{out}}(t)$  via the convolution of the input pulse  $\xi_{\text{in}}(t)$ , and channel transfer function  $h(t, z)$ , which is given by

$$\xi_{\text{out}}(t) = \xi_{\text{in}}(t) * h(t, z), \quad (19)$$

which is attributed to the non-continuous basis functions that transfer the  $q$ -number analysis into the  $c$ -number operation; the detailed derivations are given in the Supplementary Material. Note that this channel model is only used for performance analyses and simulations, and the channel model is not assumed in the security analysis.

*Simulation results.*—Based on the protocol developed, analysis scenarios, including SNU calibration, quadrature measurement, clock synchronization, sampling position, and dispersion, can be directly analyzed in the analysis of CV-QKD, as shown in Fig. 2. These results show that the continuous-mode situation has a great impact on the key rate. In addition, significant attention should be given to high-speed systems since the security issues resulting from short-pulse propagation; moreover, the sam-

pling process cannot be neglected, and improper analysis may destroy the security of the entire system.

*Conclusions.*—In this study, we have demonstrated that CV-QKD can achieve security transmission even under the assumption of a continuous mode, which is a significant step in filling the security analysis of CV-QKD. This work breaks the deadlock regarding the mismatch between CV-QKD theory and experiments, making the overall analysis framework compatible with optic-fiber communication; therefore, by calibrating the receiver and defining proper TMs, QKD can be completely realized by classical telecom components, and numerous classical communication techniques can be adopted based on this work. Many time-dependent issues, including pulse propagation, band-limited detection, sampling, and digital processing, are solved by TM descriptions, which can guide the design of high-speed long-distance experiments. In addition, our analysis indicates the significant potential of digital CV-QKD for robust and cost-effective applications. Accordingly, the analysis tools developed in this work may provide perspective for large-scale quantum-secure networks.

This work was supported by the National Natural Science Foundation of China (Grants Nos. 61531003 and 62001041), China Postdoctoral Science Foundation (Grant No. 2020TQ0016), and State Key Laboratory of Information Photonics and Optical Communications.

- 
- [1] N. Gisin, G. Ribordy, W. Tittel, H. Zbinden, Quantum cryptography, *Rev. Mod. Phys.* **74**, 145 (2002).
  - [2] S. Pirandola, U. L. Andersen, L. Banchi, M. Berta, D. Bunandar, R. Colbeck, D. Englund, T. Gehring, C. Lupo, C. Ottaviani, J. L. Pereira, M. Razavi, J. S. Shaari, M. Tomamichel, V. C. Usenko, G. Vallone, P. Villoresi, P. Wallden, Advances in quantum cryptography, *Adv. Opt. Photon.* **12**, 1012 (2020).
  - [3] F. Xu, X. Ma, Q. Zhang, H.-K. Lo, J.-W. Pan, Secure quantum key distribution with realistic devices, *Rev. Mod. Phys.* **92**, 025002 (2020).
  - [4] Q. Zhang, F. Xu, Y.-A. Chen, C.-Z. Peng, J.-W. Pan, Large scale quantum key distribution: challenges and solutions, *Opt. Express* **26**, 24260 (2018).
  - [5] M. Peev *et al.*, The SECOQC quantum key distribution network in vienna, *New J. Phys.* **11**, 075001 (2009).
  - [6] Y. Mao, B.-X. Wang, C. Zhao, G. Wang, R. Wang, H. Wang, F. Zhou, J. Nie, Q. Chen, Y. Zhao, Q. Zhang, J. Zhang, T.-Y. Chen, J.-W. Pan, Integrating quantum key distribution with classical communications in backbone fiber network, *Opt. Express* **26**, 6010 (2018).
  - [7] N. Hosseinidehaj, Z. Babar, R. Malaney, S. X. Ng, L. Hanzo, Satellite-based continuous-variable quantum communications: State-of-the-art and a predictive outlook, *IEEE Communications Surveys Tutorials* **21**, 881 (2019).
  - [8] J. F. Dynes, A. Wonfor, W. W. S. Tam, A. W. Sharpe, R. Takahashi, M. Lucamarini, A. Plews, Z. L. Yuan, A. R. Dixon, J. Cho, Y. Tanizawa, J. P. Elbers, H. Greißer, I. H. White, R. V. Penty, A. J. Shields, Cambridge quantum network, *npj Quantum Inf.* **5**, 101 (2019).
  - [9] S. K. Joshi, D. Aktas, S. Wengerowsky, M. Lončarić, S. P. Neumann, B. Liu, T. Scheidl, G. C. Lorenzo, Ž. Samec, L. Kling, A. Qiu, M. Razavi, M. Stipčević, J. G. Rarity, R. Ursin, A trusted node-free eight-user metropolitan quantum communication network, *Sci. Adv.* **6**, eaba0959 (2020).
  - [10] T. K. Paraíso, T. Roger, D. G. Marangon, I. D. Marco, M. Sanzaro, R. I. Woodward, J. F. Dynes, Z. Yuan, A. J. Shields, A photonic integrated quantum secure communication system, *Nat. Photon.* **15**, 850 (2021).
  - [11] Y.-A. Chen, Q. Zhang, T.-Y. Chen, W.-Q. Cai, S.-K. Liao, J. Zhang, K. Chen, J. Yin, J.-G. Ren, Z. Chen, S.-L. Han, Q. Yu, K. Liang, F. Zhou, X. Yuan, M.-S. Zhao, T.-Y. Wang, X. Jiang, L. Zhang, W.-Y. Liu, Y. Li, Q. Shen, Y. Cao, C.-Y. Lu, R. Shu, J.-Y. Wang, L. Li, N.-L. Liu, F. Xu, X.-B. Wang, C.-Z. Peng, J.-W. Pan, An integrated space-to-ground quantum communication network over 4,600 kilometres, *Nature* **589**, 214 (2021).
  - [12] C. Weedbrook, S. Pirandola, R. García-Patrón, N. J. Cerf, T. C. Ralph, J. H. Shapiro, S. Lloyd, Gaussian quantum information, *Rev. Mod. Phys.* **84**, 621(2012).
  - [13] E. Diamanti, A. Leverrier, Distributing secret keys with quantum continuous variables: Principle, security and implementations, *Entropy* **17**, 6072 (2015).
  - [14] F. Laudenbach, C. Pacher, C.-H. F. Fung, A. Poppe, M. Peev, B. Schrenk, M. Hentschel, P. Walther, H. Hübel, Continuous-variable quantum key distribution with gaussian modulation—the theory of practical implementations, *Adv. Quantum Technol.* **1**, 1800011 (2018).
  - [15] F. Grosshans, P. Grangier, Continuous variable quantum cryptography using coherent states, *Phys. Rev. Lett.* **88**, 057902 (2002).
  - [16] M. Navascués, F. Grosshans, A. Acín, Optimality of Gaussian attacks in continuous-variable quantum cryptography, *Phys. Rev. Lett.* **97**, 190502 (2006).
  - [17] R. García-Patrón, N. J. Cerf, Unconditional optimality of Gaussian attacks against continuous-variable quantum key distribution, *Phys. Rev. Lett.* **97**, 190503 (2006).
  - [18] F. Furrer, T. Franz, M. Berta, A. Leverrier, V. B. Scholz, M. Tomamichel, R. F. Werner, Continuous variable quantum key distribution: Finite-key analysis of composable security against coherent attacks, *Phys. Rev. Lett.* **109**, 100502 (2012).
  - [19] A. Leverrier, Composable security proof for continuous variable quantum key distribution with coherent states, *Phys. Rev. Lett.* **114**, 070501 (2015).
  - [20] A. Leverrier, Security of continuous-variable quantum key distribution via a Gaussian de Finetti reduction, *Phys. Rev. Lett.* **118**, 200501 (2017).
  - [21] S. Pirandola, Limits and security of free-space quantum communications, *Phys. Rev. Research* **3**, 013279 (2021).
  - [22] S. Pirandola, Composable security for continuous variable quantum key distribution: Trust levels and practical key rates in wired and wireless networks, *Phys. Rev. Research* **3**, 043014 (2021).
  - [23] F. Grosshans, G. V. Assche, J. Wenger, R. Brouri, N. J. Cerf, P. Grangier, Quantum key distribution using Gaussian-modulated coherent states, *Nature* **421**, 238 (2003).
  - [24] P. Jouguet, S. Kunz-Jacques, A. Leverrier, P. Grangier, E. Diamanti, Experimental demonstration of long-distance continuous-variable quantum key distribution, *Nat. Photon.* **7**, 378 (2013).
  - [25] D. Huang, P. Huang, D. Lin, G. Zeng, Long-distance continuous-variable quantum key distribution by control-

- ling excess noise, *Sci. Rep.* **6**, 19201 (2016).
- [26] Y. Zhang, Z. Li, Z. Chen, C. Weedbrook, Y. Zhao, X. Wang, Y. Huang, C. Xu, X. Zhang, Z. Wang, M. Li, X. Zhang, Z. Zheng, B. Chu, X. Gao, N. Meng, W. Cai, Z. Wang, G. Wang, S. Yu, H. Guo, Continuous-variable QKD over 50 km commercial fiber, *Quantum Sci. Technol.* **4**, 035006 (2019).
- [27] Y. Zhang, Z. Chen, S. Pirandola, X. Wang, C. Zhou, B. Chu, Y. Zhao, B. Xu, S. Yu, H. Guo, Long-distance continuous-variable quantum key distribution over 202.81 km of fiber, *Phys. Rev. Lett.* **125**, 010502 (2020).
- [28] H. Wang, Y. Pi, W. Huang, Y. Li, Y. Shao, J. Yang, J. Liu, C. Zhang, Y. Zhang, B. Xu, High-speed Gaussian-modulated continuous-variable quantum key distribution with a local local oscillator based on pilot-tone-assisted phase compensation, *Opt. Express* **28**, 32882 (2020).
- [29] F. Karinou, H. H. Brunner, C.-H. F. Fung, L. C. Comandar, S. Bettelli, D. Hillerkuss, M. Kuschnerov, S. Mikroulis, D. Wang, C. Xie, M. Peev, A. Poppe, Toward the integration of CV quantum key distribution in deployed optical networks, *IEEE Photon. Technol. Lett.* **30**, 650 (2018).
- [30] T. A. Eriksson, T. Hirano, B. J. Puttnam, G. Rademacher, R. S. Luís, M. Fujiwara, R. Namiki, Y. Awaji, M. Takeoka, N. Wada, M. Sasaki, Wavelength division multiplexing of continuous variable quantum key distribution and 18.3 Tbit/s data channels, *Commun. Phys.* **2**, 9 (2019).
- [31] T. A. Eriksson, R. S. Luís, B. J. Puttnam, G. Rademacher, M. Fujiwara, Y. Awaji, H. Furukawa, N. Wada, M. Takeoka, M. Sasaki, Wavelength division multiplexing of 194 continuous variable quantum key distribution channels, *J. Lightwave Technol.* **38**, 2214 (2020).
- [32] S. Ghorai, P. Grangier, E. Diamanti, and A. Leverrier, Asymptotic Security of Continuous-Variable Quantum Key Distribution with a Discrete Modulation, *Phys. Rev. X* **9**, 021059 (2019).
- [33] J. Lin, T. Upadhyaya, and N. Lütkenhaus, Asymptotic Security Analysis of Discrete-Modulated Continuous-Variable Quantum Key Distribution, *Phys. Rev. X* **9**, 041064 (2019).
- [34] K. J. Blow, R. Loudon, S. J. D. Phoenix, T. J. Shepherd, Continuum fields in quantum optics, *Phys. Rev. A* **42**, 4102 (1990).
- [35] C. Fabre and N. Treps, Modes and States in Quantum Optics, *Rev. Mod. Phys.* **92**, 40 (2020).
- [36] M. G. Raymer and I. A. Walmsley, Temporal Modes in Quantum Optics: Then and Now, *Phys. Scr.* **95**, 064002 (2020).
- [37] See the Supplemental Material for the basic concept of continuous-mode CV-QKD, which includes Refs. [2–4, 7, 42].
- [38] M. G. Raymer, Z. W. Li, and I. A. Walmsley, Temporal Quantum Fluctuations in Stimulated Raman Scattering: Coherent-Modes Description, *Phys. Rev. Lett.* **63**, 1586 (1989).
- [39] C. M. Caves and B. L. Schumaker, New Formalism for Two-Photon Quantum Optics. I. Quadrature Phases and Squeezed States, *Phys. Rev. A* **31**, 3068 (1985).
- [40] D. J. Santos, R. Loudon, and F. J. Fraile-Peláez, Continuum States and Fields in Quantum Optics, *Am. J. Phys.* **65**, 126 (1997).
- [41] J. R. Jeffers, N. Imoto, and R. Loudon, Quantum Optics of Traveling-Wave Attenuators and Amplifiers, *Phys. Rev. A* **47**, 3346 (1993).
- [42] M. J. Collett, R. Loudon, and C. W. Gardiner, Quantum Theory of Optical Homodyne and Heterodyne Detection, *J. Mod. Opt.* **34**, 881 (1987).

## Supplementary material for “Digital Quantum Key Distribution with Continuous-Mode Formalism”

In this Supplemental material, we provide additional details on the continuous-mode continuous variable quantum key distribution (CV-QKD) protocol. We first introduce the form of source model with continuous-mode formalism. Then, we give a model of time-dependent measurement in CV-QKD. Next, the statistics of measurement results used for key rate calculations are given. The generalized channel model is illustrated and finally, the entanglement-based scheme is introduced.

### SOURCE MODEL

In this section, we introduce the source model of the proposed continuous-mode CV-QKD protocol. Continuous-mode operators are introduced, followed by field-operator and temporal-mode descriptions. Finally, continuous-mode coherent states used in CV-QKD are illustrated.

#### Continuous-mode operators

In this work, we focus on time-dependent coherent state transmission scenarios in continuous-variable quantum cryptography, such as pulsed signals and encoded quantum states; different toolboxes are considered than those used in single-mode continuous-wave (CW) electric field cases. Continuous-mode operators in the time domain are powerful tools for addressing this kind of issue.

Consider that a one-dimensional optical cavity of length  $L$  is exploited to generate optical modes. Discrete- and continuous-mode operators can then be defined based on the second quantization process [1]. In discrete-mode cases, the interval of the wave vectors of the plane waves traveling in the cavity is given by [2, 3]

$$\Delta k = \frac{2\pi}{L}, \quad (20)$$

and the corresponding eigenfrequency and mode spacing are given by

$$\Delta\omega = \frac{2\pi c}{L}. \quad (21)$$

Thus, the output frequencies of different running waves in the cavity should be integral multiples of the longitudinal mode spacing, as follows:

$$\Delta\omega_i = n_i \frac{2\pi c}{L}. \quad (22)$$

For every discrete mode in the cavity labeled by  $i, j$ , the electric field is described by creation and annihilation operators in terms of discrete cases (given by  $\hat{a}_i^\dagger, \hat{a}_i$ ) that satisfy a boson commutation relation, which is given by

$$[\hat{a}_i, \hat{a}_j^\dagger] = \delta_{ij}, \quad (23)$$

where  $\delta_{ij}$  is the Kronecker delta tensor.

As the cavity length approaches infinity, the spacing between modes becomes narrow, which means that  $L \rightarrow \infty, \Delta\omega \rightarrow 0$ ; then, the discrete-mode operator becomes the continuous-mode operator. To ensure energy conservation before and after the transformation, we have the following correspondence:

$$\hat{a}_i \rightarrow (\Delta\omega)^{\frac{1}{2}} \hat{a}(\omega), \quad (24)$$

and the Kronecker delta tensor becomes the Dirac delta function, which is given by

$$\delta_{ij} \rightarrow \Delta\omega \delta(\omega - \omega'). \quad (25)$$

Discrete sums are converted to continuous integrals:

$$\sum_i \rightarrow \frac{1}{\Delta\omega} \int d\omega. \quad (26)$$



From the above correspondence, it can be deduced that the continuous-mode creation and annihilation operators satisfy the following commutation relation:

$$[\hat{a}(\omega), \hat{a}^\dagger(\omega')] = \delta(\omega - \omega'). \quad (27)$$

In that case, the positive frequency part of a continuous-mode electric field can be described in terms of the continuous-mode operators, which reads as

$$\hat{E}^+(z, t) = i \int d\omega \mathcal{E}(\omega) \hat{a}(\omega) \exp \left[ -i\omega \left( t - \frac{z}{c} \right) \right], \quad (28)$$

where  $\mathcal{E}$  is the dimensionality of an electric field, and the overall electric field is given by

$$\hat{E}(z, t) = \hat{E}^+(z, t) + h.c., \quad (29)$$

where  $h.c.$  denotes the hermitian conjugation.

In time evolution scenarios, especially when the measured signals are pulses, it is always useful to define the Fourier transforms of continuous-mode field operators in the time domain; this is given by

$$\hat{a}(t) = \frac{1}{\sqrt{2\pi}} \int d\omega \hat{a}(\omega) \exp(-i\omega t). \quad (30)$$

It can be proven that the continuous-mode operator in the time domain satisfies the following commutation relation:

$$[\hat{a}(t), \hat{a}^\dagger(t')] = \delta(t - t'). \quad (31)$$

### Field-operator and non-continuous basis descriptions

Field operators and non-continuous basis functions offer a powerful method to analyze pulse or other time-dependent transmission scenarios.

In continuous-mode cases, it is assumed that a vacuum state exists in every single mode; such a state can be defined as

$$|\{0\}\rangle = |0\rangle, \quad (32)$$

and we also have

$$\hat{a}(\omega) |0\rangle = 0. \quad (33)$$

With the help of vacuum states, any quantum states can be defined by creating photons from vacuum states, as follows [4]:

$$|\Psi_\omega\rangle = \hat{a}^\dagger(\omega) |0\rangle. \quad (34)$$

In the above definition, the generated states cannot be well normalized, which is inconvenient for subsequent analysis. To facilitate the subsequent analysis, we use the infinitely countable complete orthonormal set of functions  $\{\xi_i(\omega)\}_{i=1}^\infty$  to simplify the analysis. This set of functions obeys the following relations:

$$\sum_{i=1}^\infty \xi_i(\omega) \xi_i^*(\omega') = \delta(\omega - \omega'), \quad (35)$$

$$\int d\omega \xi_i(\omega) \xi_j^*(\omega) = \delta_{ij}. \quad (36)$$

If a new set of quantum states  $\{|\psi(\xi_i)\rangle\}_{i=1}^\infty$  on  $\xi_i$  on  $\xi_i$  is considered, it can be expressed as the superposition of the nonnormalized state  $|\Psi_\omega\rangle$  defined in Eq. (34), which is written as

$$|\psi(\xi_i)\rangle = \int d\omega \xi_i(\omega) |\Psi_\omega\rangle = \int d\omega \xi_i(\omega) \hat{a}^\dagger(\omega) |0\rangle. \quad (37)$$

Based on the properties of  $\xi_i(\omega)$ ,  $|\psi(\xi_i)\rangle$  can be well normalized. According to the above properties,  $|\psi(\xi_i)\rangle$  can be regarded as a continuous-mode operator  $\hat{A}^\dagger(\xi_i)$  acting on the vacuum states, and  $\hat{A}^\dagger(\xi_i)$  is defined as

$$\hat{A}^\dagger(\xi_i) = \int d\omega \xi_i(\omega) \hat{a}^\dagger(\omega), \quad (38)$$

which denotes the “field operator” or the photon wave-packet creation operator in quantum field theory; this means that a quantum state with an envelope  $\xi_i(\omega)$  is generated at position  $\omega$ , where  $\xi_i(\omega)$  is the envelope of the created wave packet.

By using the commutation relation between  $\hat{a}(\omega)$  and  $\hat{a}^\dagger(\omega)$  shown in Eq. (27), it can be proven that  $\hat{A}^\dagger(\xi_i)$  and  $\hat{A}(\xi_i)$  satisfy the following discrete bosonic commutation relations:

$$[\hat{A}(\xi_i), \hat{A}^\dagger(\xi_j)] = \delta_{ij}, \quad (39)$$

$$[\hat{A}(\xi_i), \hat{A}(\xi_i)] = [\hat{A}^\dagger(\xi_i), \hat{A}^\dagger(\xi_i)] = 0. \quad (40)$$

Consequently, the operator  $\hat{a}(\omega)$  can be rewritten as a superposition of the field operators, given by

$$\hat{a}(\omega) = \sum_i \xi_i(\omega) \hat{A}(\xi_i). \quad (41)$$

To facilitate discussion in the case of pulsed signals, the field operators in the frequency domain can be expressed in an equivalent time-domain form. The inverse Fourier transform converts the envelope  $\xi_i(\omega)$  in the frequency domain to an envelope  $\xi_i(t)$  in the time domain, given by

$$\xi_i(t) = \frac{1}{\sqrt{2\pi}} \int d\omega \xi_i(\omega) \exp(-i\omega t), \quad (42)$$

and the field creation operator in the time domain can also be obtained by the Fourier transform of Eq. (41), which takes the form

$$\hat{A}^\dagger(\xi_i) = \int dt \xi_i(t) \hat{a}^\dagger(t). \quad (43)$$

The continuous-mode operator  $\hat{a}(t)$  can be finally expressed as a superposition of the field operators on behalf of the non-continuous basis functions:

$$\hat{a}(t) = \sum_i \xi_i(t) \hat{A}(\xi_i). \quad (44)$$

The scenario of pulse generation via a continuous-mode operator and non-continuous basis functions is shown in Fig. 3. The expansion of the continuous-mode operator in the time domain, as shown in Eq. (44), is illustrated in Fig. 3 (a), and its Fourier transform (shown in Eq. (41)) is given in Fig. 3 (b). These two forms are crucial in analyzing pulse propagation and band-limited scenarios.

It can be seen that in pulse transmission cases, the forms of non-continuous basis functions can change the complex  $q$ -number analysis process into simple  $c$ -number processing, which simplifies the analysis to a large extent.

### Continuous-mode coherent states

Similar to single-mode cases, the definition of a continuous-mode coherent state is still a displacement operator acting on the vacuum state:

$$|\{\alpha(\omega)\}\rangle := \hat{D}(\alpha(\omega)) |0\rangle, \quad (45)$$

where

$$\hat{D}(\alpha(\omega)) = \exp \left[ \int d\omega [\alpha(\omega) \hat{a}^\dagger(\omega) - \alpha^*(\omega) \hat{a}(\omega)] \right] \quad (46)$$

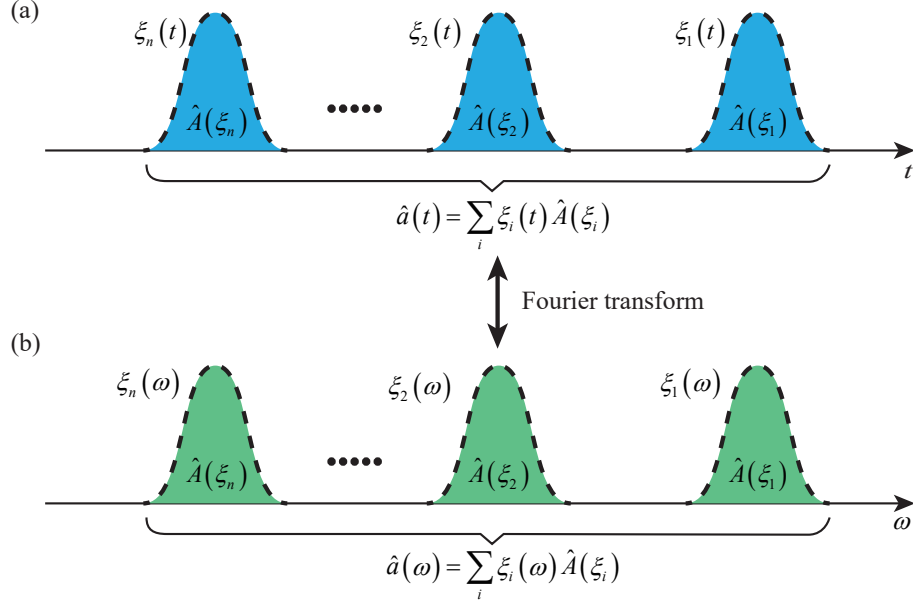


FIG. 3. Pulse propagation scenario via non-continuous basis functions. (a) The expansion of the continuous-mode operator in the time domain. (b) The expansion of the continuous-mode operator in the frequency domain. These two scenarios are Fourier transform pair.

is the displacement operator, and the continuous-mode coherent state is given by

$$|\{\hat{a}(\omega)\}\rangle = |\hat{a}_1(\omega)\rangle \otimes \dots \otimes |\hat{a}_i(\omega)\rangle \otimes \dots \quad (47)$$

According to this definition, it is easy to prove that the continuous-mode coherent state is the eigenstate of the annihilation operator, for which the eigenvalue equation is given by

$$\hat{a}(\omega) |\{\alpha(\omega)\}\rangle = \alpha(\omega) |\{\alpha(\omega)\}\rangle. \quad (48)$$

According to Eq. (45), the continuous-mode coherent state can also be described in a time-dependent form, which is given by

$$|\{\alpha(\omega)\}\rangle = |\{\alpha(t)\}\rangle = \hat{D}(\alpha(t)) |0\rangle, \quad (49)$$

and the eigenvalue equation is

$$\hat{a}(t) |\{\alpha(t)\}\rangle = \alpha(t) |\{\alpha(t)\}\rangle. \quad (50)$$

The calculation of the continuous-mode operator is complex in many cases, especially if the  $q$ -number equation appears when the pulse propagates. To convert the  $q$ -number equation into a  $c$ -number equation, one option is to expand it by exploiting a set of non-continuous basis functions. The displacement operator is then rewritten as

$$\begin{aligned} \hat{D}(\alpha(\omega)) &= \exp \left[ \int d\omega [\alpha(\omega) \hat{a}^\dagger(\omega) - \alpha^*(\omega) \hat{a}(\omega)] \right] \\ &= \exp \left\{ \sum_i [\gamma_i \hat{A}^\dagger(\xi_i) - \gamma_i^* \hat{A}(\xi_i)] \right\}, \end{aligned} \quad (51)$$

where

$$\gamma_i = \int d\omega \alpha(\omega) \xi_i^*(\omega) \quad (52)$$

denotes a parameter of a continuous-mode coherent state under a non-continuous basis. Therefore, the coherent state

represented by a set of non-continuous basis functions is given by

$$\begin{aligned}
|\{\alpha(\omega)\}\rangle &= \hat{D}(\alpha(\omega))|0\rangle \\
&= \exp\left\{\sum_i \left[\gamma_i \hat{A}^\dagger(\xi_i) - \gamma_i^* \hat{A}(\xi_i)\right]\right\}|0\rangle \\
&= \prod_i |\gamma_i\rangle = |\{\gamma_i\}\rangle.
\end{aligned} \tag{53}$$

A single wave-packet coherent state  $|\gamma_i\rangle$  is the eigenstate of  $\hat{A}(\xi_i)$ , which is described by

$$\hat{A}(\xi_i)|\gamma_i\rangle = \gamma_i|\gamma_i\rangle. \tag{54}$$

Therefore the overall sequence of continuous-mode coherent state can be written as

$$\begin{aligned}
\hat{a}(\omega)|\{\alpha(\omega)\}\rangle &= \sum_i \xi_i(\omega) \hat{A}(\xi_i)|\{\gamma_i\}\rangle \\
&= \sum_i \xi_i(\omega) \gamma_i |\{\gamma_i\}\rangle.
\end{aligned} \tag{55}$$

Thus, the eigenvalues of continuous-mode operators can be expressed as linear combinations of discrete eigenvalues, as follows:

$$\alpha(\omega) = \sum_i \xi_i(\omega) \gamma_i. \tag{56}$$

Similarly, the sequence of pulsed coherent states in the time domain can be written as

$$\begin{aligned}
\hat{a}(t)|\{\alpha(t)\}\rangle &= \sum_i \xi_i(t) \hat{A}(\xi_i)|\{\gamma_i\}\rangle \\
&= \sum_i \xi_i(t) \gamma_i |\{\gamma_i\}\rangle.
\end{aligned} \tag{57}$$

The eigenvalues of continuous operators can be obtained as follows:

$$\alpha(t) = \sum_i \xi_i(t) \gamma_i, \tag{58}$$

and  $|\xi_i|^2$  is the mean photon number in each pulse. Eq. (57) is the generalized equation for addressing pulsed coherent state issues.

## MEASUREMENT MODEL

In this section, we introduce the measurement model of the proposed continuous-mode CV-QKD protocol. We describe continuous-mode detection in the time domain first, and then the frequency domain and quadrature descriptions are considered, respectively. Finally, the sampling model is given to derive the measured results.

### Time domain description with impulse response function

Homodyne detection is always used in CV-QKDs to detect the quadratures of the measured quantum states. The analysis of ideal homodyne detection in the single-mode case has been very frequently used in CV-QKD, while this work focuses on the time-dependent measurement process. A general homodyne detection method is shown in Fig. 4.

In Fig. 4, it can be seen that the signal and the local oscillator (LO) with continuous-mode forms are inputted into the homodyne detector, and after a balanced beam splitter, the output signals are detected by two photodetectors.

The continuous-mode form of homodyne detection can deal with both time-dependent and frequency-dependent cases, including CW signals and pulsed signals.



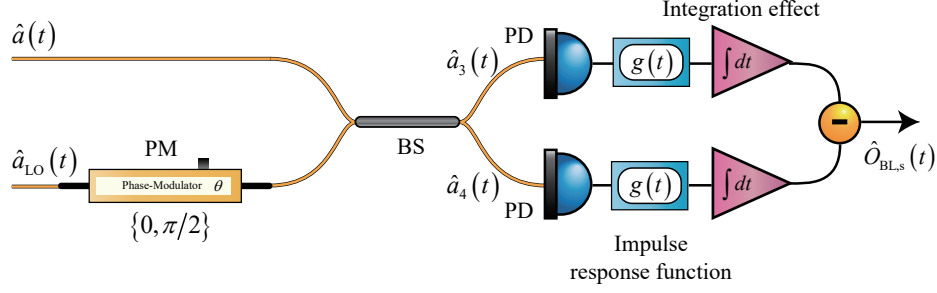


FIG. 4. A general homodyne detection model. PM: phase modulator; BS: beam splitter; PD: photodetector.

In the time domain, first, ignoring the bandwidth of the photodetector (PD), the instantaneous flux operator,  $\hat{f}(t)$ , measured in photon per unit time is given by

$$\hat{f}(t) = \hat{a}^\dagger(t) \hat{a}_{\text{LO}}(t) + \hat{a}_{\text{LO}}^\dagger(t) \hat{a}(t), \quad (59)$$

where  $\hat{a}(t)$  and  $\hat{a}_{\text{LO}}(t)$  denote the annihilation operators of the measured signal and the LO at instantaneous time  $t$ , respectively. By the integral of flux operator, the output photocurrent operator after homodyne detection can be written in a time-dependent form, which is given by

$$\hat{O}(t) = \int_t^{t+T} dt \left[ \hat{a}^\dagger(t) \hat{a}_{\text{LO}}(t) + \hat{a}_{\text{LO}}^\dagger(t) \hat{a}(t) \right], \quad (60)$$

where  $T$  is the integration time of a PD.

Now, let us investigate an instantaneous one-shot measurement considering the pulse shapes. A single wave-packet operator given in Eq. (44) is introduced, and the signal's and the LO's operators are expressed as

$$\hat{a}(t) = \xi(t) \hat{A}(\xi), \quad (61)$$

$$\hat{a}_{\text{LO}}(t) = \xi_{\text{LO}}(t) \hat{A}_{\text{LO}}(\xi_{\text{LO}}). \quad (62)$$

By combining Eqs. (60-62), the photocurrent operator is rewritten as

$$\hat{O}(t) = \int_t^{t+T} dt \left[ \xi^*(t) \xi_{\text{LO}}(t) \hat{A}^\dagger(\xi) \hat{A}_{\text{LO}}(\xi_{\text{LO}}) + \xi_{\text{LO}}^*(t) \xi(t) \hat{A}_{\text{LO}}^\dagger(\xi_{\text{LO}}) \hat{A}(\xi) \right] \quad (63)$$

$$= \int_t^{t+T} dt (\xi^*(t) \xi_{\text{LO}}(t)) \hat{A}^\dagger(\xi) \hat{A}_{\text{LO}}(\xi_{\text{LO}}) + \int_t^{t+T} dt (\xi_{\text{LO}}^*(t) \xi(t)) \hat{A}_{\text{LO}}^\dagger(\xi_{\text{LO}}) \hat{A}(\xi), \quad (64)$$

where  $\xi(t)$  and  $\xi_{\text{LO}}(t)$  are dimensionless complex numbers. We can see that from Eq. (64), the photocurrent operator contains both the classical envelope information ( $\xi^*(t) \xi_{\text{LO}}(t)$  and  $\xi_{\text{LO}}^*(t) \xi(t)$ ) and the quantum operator information ( $\hat{A}^\dagger(\xi) \hat{A}_{\text{LO}}(\xi_{\text{LO}})$  and  $\hat{A}_{\text{LO}}^\dagger(\xi_{\text{LO}}) \hat{A}(\xi)$ ). In one wave packet, the quantum operator part is invariant, so the time evolution can be simply reflected in the classical wave packet.

Then, the limited bandwidth is considered. Assume that detector's impulse response function is given by  $g(t)$ , and  $g(t)$  is a dimensionless complex number. The band-limited photocurrent operator  $\hat{O}_{\text{BL}}(t)$  is given by

$$\begin{aligned} \hat{O}_{\text{BL}}(t) &= \hat{O}(t) * g(t) \\ &= \int_t^{t+T} dt \left[ \hat{a}^\dagger(t) \hat{a}_{\text{LO}}(t) + \hat{a}_{\text{LO}}^\dagger(t) \hat{a}(t) \right] * g(t) \end{aligned} \quad (65)$$

$$= \int_t^{t+T} dt \left[ \xi^*(t) \xi_{\text{LO}}(t) \hat{A}^\dagger(\xi) \hat{A}_{\text{LO}}(\xi_{\text{LO}}) + \xi_{\text{LO}}^*(t) \xi(t) \hat{A}_{\text{LO}}^\dagger(\xi_{\text{LO}}) \hat{A}(\xi) \right] * g(t) \quad (66)$$

$$= \int_t^{t+T} dt [(\xi^*(t) \xi_{\text{LO}}(t)) * g(t)] \hat{A}^\dagger(\xi) \hat{A}_{\text{LO}}(\xi_{\text{LO}}) + \int_t^{t+T} dt [(\xi_{\text{LO}}^*(t) \xi(t)) * g(t)] \hat{A}_{\text{LO}}^\dagger(\xi_{\text{LO}}) \hat{A}(\xi). \quad (67)$$

We can see the powerful ability of the non-continuous basis function, which directly transforms our continuous-mode analysis into the treatment of classical wave packets, while the quantum operator part does not be involved.

### Frequency domain description with frequency response functions

Recall that the instantaneous flux operator  $\hat{f}(t)$  in the time domain is given by Eq. (59). In the frequency domain, the spectrum of output current  $\hat{f}(\omega)$  is given by

$$\begin{aligned}\hat{f}(\omega) &= \mathcal{F}(\hat{f}(t)) \\ &= \frac{1}{\sqrt{2\pi}} \int dt \hat{f}(t) \exp(i\omega t), \\ &= \hat{a}^\dagger(\omega) * \hat{a}_{\text{LO}}(\omega) + \hat{a}_{\text{LO}}^\dagger(\omega) * \hat{a}(\omega),\end{aligned}\quad (68)$$

where  $\mathcal{F}(\cdot)$  denotes the Fourier transfer, and

$$A(x) * B(x) = \int_{-\infty}^{\infty} d\tau A(\tau) B(x - \tau) \quad (69)$$

is the convolution of  $A(x)$  and  $B(x)$ . After considering the band-limited detection model, the complete description can be given by two subtracted photodetectors with limited bandwidth and integration effect, as shown in Fig. 4.

By the Fourier transform of the signal's and the LO's operators shown in Eqs.(61,62), the operators in the frequency domain are given by

$$\hat{a}(\omega) = \xi(\omega) \hat{A}(\xi), \quad (70)$$

$$\hat{a}_{\text{LO}}(\omega) = \xi_{\text{LO}}(\omega) \hat{A}_{\text{LO}}(\xi_{\text{LO}}), \quad (71)$$

where  $\xi(\omega)$  and  $\xi_{\text{LO}}(\omega)$  are the spectra of the quantum signal and the LO respectively. By combing Eqs. (68-71), the flux operator in the frequency domain is rewritten as

$$\begin{aligned}\hat{f}(\omega) &= \left( \xi^*(-\omega) \hat{A}^\dagger(\xi) \right) * \left( \xi_{\text{LO}}(\omega) \hat{A}_{\text{LO}}(\xi_{\text{LO}}) \right) + \left( \xi_{\text{LO}}^*(-\omega) \hat{A}_{\text{LO}}^\dagger(\xi_{\text{LO}}) \right) * \left( \xi(\omega) \hat{A}(\xi) \right) \\ &= \xi^*(-\omega) * \xi_{\text{LO}}(\omega) \hat{A}^\dagger(\xi) \hat{A}_{\text{LO}}(\xi_{\text{LO}}) + \xi_{\text{LO}}^*(-\omega) * \xi(\omega) \hat{A}_{\text{LO}}^\dagger(\xi_{\text{LO}}) \hat{A}(\xi),\end{aligned}\quad (72)$$

where we use the relation  $\mathcal{F}[X^*(t)] = \tilde{X}^*(-\omega)$ .

To take the bandwidth of detectors into consideration, here, we investigate detailed detection processes of one PD. Assume that the frequency response transfer function of one detector is  $\tilde{G}(\omega)$ , which is the Fourier transform of the impulse response function  $g(t)$ . After subtraction between two output currents, the band-limited flux operator after band-limited homodyne detection can be written as

$$\begin{aligned}\hat{f}_{\text{BL}}(\omega) &= \hat{f}(\omega) \tilde{G}(\omega) \\ &= (\xi^*(-\omega) * \xi_{\text{LO}}(\omega)) \tilde{G}(\omega) \hat{A}^\dagger(\xi) \hat{A}_{\text{LO}}(\xi_{\text{LO}}) + (\xi_{\text{LO}}^*(-\omega) * \xi(\omega)) \tilde{G}(\omega) \hat{A}_{\text{LO}}^\dagger(\xi_{\text{LO}}) \hat{A}(\xi).\end{aligned}\quad (73)$$

The result shown in Eq. (73) is the Fourier transform of the time domain form, which makes it easier to analyze spectrum-related problems. A more intuitive way to understand the band-limited detection model can be summarized in Fig. 5. For general band-limited scenarios, only classical terms need to be considered first, and then the wide-spectrum quantum operators is calculated.

Now, using the band-limited detection model, we can take the spectrum of sources into consideration. Let us consider the band-limited detection process in detail. We can divide the whole measurement process into the following parts, as shown in the Fig. 5:

Step 1: *Defining band-limited operator.* The band-limited operator is decomposed into the product of the wave-packet creation operator and the spectral envelope, given by Eq. (70), where the wave-packet creation operator reflects the quantum character, and the spectral envelope embodies the classical character of the state.

Step 2: *Displacement.* For easier analysis of spectral effects, we define the high frequency spectrum  $\xi(\omega)$  as the shift of the low frequency spectrum  $\xi_0(\omega)$ . Either the spectrum of signals or the spectrum of LOs can be obtained by displacing the baseband spectrum to high frequencies and the spectra of quantum signals and LOs can be respectively given by

$$\xi_{\text{sig}}(\omega) = \xi_{\text{sig},0}(\omega - \omega_s) = \xi_{\text{sig},0}(\omega) * \delta(\omega - \omega_s), \quad (74)$$

$$\xi_{\text{LO}}(\omega) = \xi_{\text{LO},0}(\omega - \omega_{\text{LO}}) = \xi_{\text{LO},0}(\omega) * \delta(\omega - \omega_{\text{LO}}), \quad (75)$$

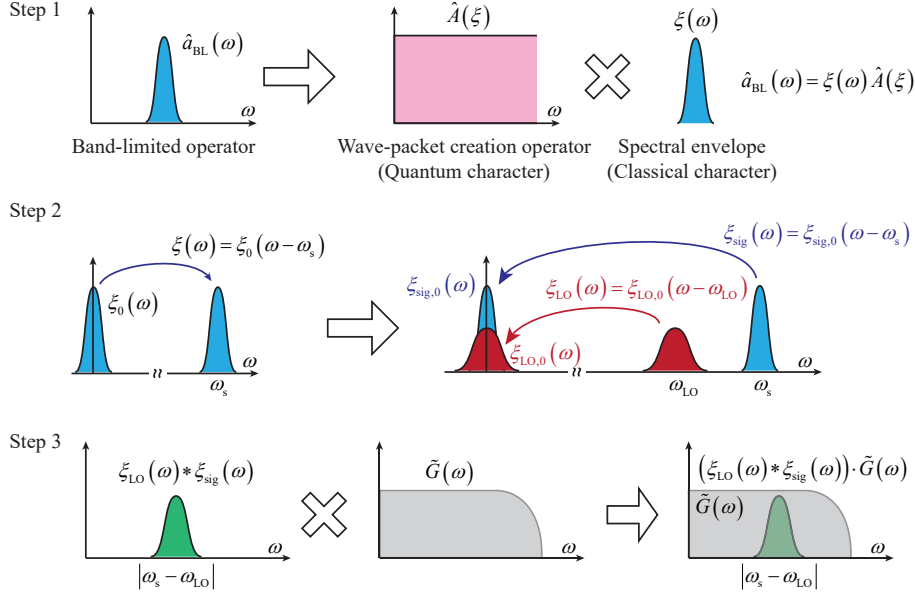


FIG. 5. Band-limited operator and the the measurement process via the band-limited detection.

and the transfer functions in the time domain is given by

$$\begin{aligned}\xi_{sig}(t) &= \xi_{sig,0}(t) \exp(i\omega_s t), \\ \xi_{LO}(t) &= \xi_{LO,0}(t) \exp(i\omega_{LO} t).\end{aligned}\tag{76}$$

Using this notation, it is easy to discuss the signals with different center frequencies and the corresponding spectrum envelope information in the security analysis.

**Step 3: Adding PD's frequency response function.** After passing through the BS of the homodyne detection, the spectrum of the combined signal is given by  $\xi^*(-\omega) * \xi_{LO}(\omega)$ . If the spectra of the signal and the LO have the forms shown in Eqs. (74,75), the intermediate frequency (IF)  $\Delta\omega = |\omega_s - \omega_{LO}|$  emerges. The final detected spectrum is given by the convolution of PD's transfer function and previous results, as shown in Eq. (73).

The next step is to calculate the quadrature components in the time domain, which is useful to derive the secret key rate.

### Quadrature description

We can now calculate band-limited results related to signal's spectrum. By combining Eqs. (67,76), we can get the following result:

$$\begin{aligned}\hat{O}_{BL}(t) &= \int_t^{t+T} dt [(\xi_{sig,0}(t) \xi_{LO,0}(t)) * g(t)] \left[ \exp(-i\Delta\omega t) \hat{A}^\dagger(\xi) \hat{A}_{LO}(\xi_{LO}) + \exp(i\Delta\omega t) \hat{A}_{LO}^\dagger(\xi_{LO}) \hat{A}(\xi) \right] \\ &= \int_t^{t+T} dt [S_0(t) * g(t)] \left[ \exp(-i\Delta\omega t) \hat{A}^\dagger(\xi) \hat{A}_{LO}(\xi_{LO}) + \exp(i\Delta\omega t) \hat{A}_{LO}^\dagger(\xi_{LO}) \hat{A}(\xi) \right].\end{aligned}\tag{77}$$

where  $S_0(t) = \xi_{sig,0}(t) \xi_{LO,0}(t)$  denotes the joint source spectrum in terms of the baseband.

This result is consistent with the IF homodyne detection result, where non-zero frequency difference between the quantum signal and the LO is considered, especially in many local LO experiments. This result improves the previous security analysis that did not give a strict proof of IF homodyne CV-QKD.

Moreover, The spectra of signals, LOs, and the frequency response of the detector can be analyzed by this model. We can see that, the  $\exp(i\Delta\omega t)$  term is introduced by the displaced frequency difference of two spectra in the frequency domain, which directly converts the  $q$ -number operation of different modes into a simple envelope  $c$ -number operation, thereby bringing great convenience to the derivation of results. The  $S_0(t)$  term is introduced by the beating between

the quantum state and the LO, in terms of the baseband spectrum.  $g(t)$  is introduced by the detector's transfer function.

In brief, considering the influence of source and detection spectrum, the final band-limited measurement result is denoted by the convolution between the continuous-mode operator and the system's transfer function.

In many CV-QKD cases, the input quantum state is considered to be a sequence of pulsed coherent states. Before homodyne detection, the overall states fed to the input ports are given by:

$$|\psi_{\text{in}}\rangle = |\{\gamma_i\}\rangle_s \otimes |\{\mu_i\}\rangle_{\text{LO}}, \quad (78)$$

where  $|\{\gamma_i\}\rangle_s$  and  $|\{\mu_i\}\rangle_{\text{LO}}$  are the wave-packet coherent states of the signal and the LO. Assume the LO is a classical light, which has the parameter given by

$$\mu = \mu_{\text{LO}}^{1/2} \exp(-i\theta_{\text{LO}}), \quad (79)$$

where  $\mu_{\text{LO}}$  denotes the average number of photons contained in each LO pulse.  $|\{\gamma_i\}\rangle$  is the measured pulsed signal coming from the quantum channel, and  $|\gamma_i|^2$  represents the average number of photons contained in the  $i$ -th signal pulse.

In the following analysis, only one pulse is considered, and more general cases can be deduced in the same way. From Eqs. (77,79), by tracing the effect of the LO, the output photocurrent operator can be rewritten as

$$\begin{aligned} \hat{O}_{\text{BL},s}(t) &= {}_{\text{LO}} \langle \mu | \hat{O}_{\text{BL}}(t) | \mu \rangle_{\text{LO}} \\ &= \mu_{\text{LO}}^{1/2} \int_t^{t+T} dt [S_0(t) * g(t)] \left\{ \exp[i(\Delta\omega t + \theta)] \hat{A}^\dagger(\xi) + \exp[-i(\Delta\omega t + \theta)] \hat{A}(\xi) \right\} \\ &= \mu_{\text{LO}}^{1/2} \int_t^{t+T} dt [S_0(t) * g(t)] X_\xi^{\Delta\omega t + \theta}(t), \end{aligned} \quad (80)$$

where  $X_\xi^{\Delta\omega t + \theta}(t)$  denotes the quadrature operator of the input wave-packet coherent state while ignoring the pulse shape, which is given by

$$X_\xi^{\Delta\omega t + \theta}(t) = \exp[i(\Delta\omega t + \theta)] \hat{A}^\dagger(\xi) + \exp[-i(\Delta\omega t + \theta)] \hat{A}(\xi). \quad (81)$$

By defining the time-invariant in-phase component  $\hat{I}_\xi$  and the quadrature component  $\hat{Q}_\xi$  of the photon wave packet  $\xi(t)$ , which reads

$$\hat{I}_\xi = \frac{1}{2} (\hat{A}^\dagger(\xi) + \hat{A}(\xi)), \quad (82)$$

$$\hat{Q}_\xi = \frac{i}{2} (\hat{A}^\dagger(\xi) - \hat{A}(\xi)), \quad (83)$$

the quadrature operator shown is Eq. (81) is then rewritten as

$$X_\xi^{\Delta\omega t + \theta}(t) = \hat{I}_\xi \cos(\Delta\omega t + \theta) - i\hat{Q}_\xi \sin(\Delta\omega t + \theta), \quad (84)$$

and the photocurrent operator can be rewritten as

$$\hat{O}_{\text{BL},s}(t) = \mu_{\text{LO}}^{1/2} \int_t^{t+T} dt [S_0(t) * g(t)] \left[ \hat{I}_\xi \cos(\Delta\omega t + \theta) - i\hat{Q}_\xi \sin(\Delta\omega t + \theta) \right]. \quad (85)$$

### Sampling model

Assume that the sampling procedure follows the principle of integral hold, which means that the outcome after the analog-to-digital converter (ADC) is the average of the measurement results at the time interval  $[t_i, t_i + \Delta t_s]$ , where  $t_i$  is the sampling time, and  $\Delta t_s$  denotes the sampling-hold time, which is usually much less than the sampling time.



The sampled photocurrent operator is then given by

$$\hat{D}_{t_i} = \frac{1}{\Delta t_s} \int_{t_i}^{t_i + \Delta t_s} dt \hat{O}_{BL,s}(t) \quad (86)$$

$$= \frac{1}{\Delta t_s} \mu_{LO}^{1/2} \int_{t_i}^{t_i + \Delta t_s} dt \int_t^{t+T} dt' [S_0(t') * g(t')] X_\xi^{\Delta\omega t' + \theta}(t'), \quad (87)$$

Supposing the integration time  $T$  of the PD is short compared with the variation of quadrature components, Eq. (87) can be then simplified, which reads

$$\hat{D}_{t_i} = \frac{T}{\Delta t_s} \mu_{LO}^{1/2} \int_{t_i}^{t_i + \Delta t_s} dt [S_0(t) * g(t)] X_\xi^{\Delta\omega t + \theta}(t). \quad (88)$$

In one pulse,  $N$  points are usually collected, and suppose that the sampling time interval is  $T_s$ , so we can get the measurement results from an operator set, given by  $\{\hat{D}_{t_i}\}_{i=1}^N$ , and  $t_i = iT_s$ . We leave the case that the sampling-hold time  $\Delta t_s$  is comparable with the sampling time  $T_s$  for further investigations.

For the case where  $\Delta t_s \ll T_s$ , we can assume that the signal does not change within the hold time, which is intuitive in low sample rate systems, and the sampled current operator can be further simplified, which reads

$$\hat{D}_{t_i} = T \mu_{LO}^{1/2} [S_0(t) * g(t) X_\xi^{\Delta\omega t + \theta}(t)]_{t=t_i} \quad (89)$$

$$= T \mu_{LO}^{1/2} [S_0(t) * g(t)] \left[ \hat{I}_\xi \cos(\Delta\omega t + \theta) - i \hat{Q}_\xi \sin(\Delta\omega t + \theta) \right]_{t=t_i}. \quad (90)$$

We can see that from Eq. (90), the sampling results consist of the product of the envelope and the quadrature operator, where the envelope contains the classical time domain information of signals, and the quadrature operator contains the quantum information related to the measured states. The evolution of states can be fully expressed by the evolution of envelopes, thereby simplifying the analysis.

Using the techniques widely used in classical coherent optical communication [6], as shown in Fig. 6, the in-phase and quadrature components can be extracted, respectively. The output result is first multiplied by a microwave LO whose phase is aligned with that of the IF signal, and then passes a low-pass filter. This procedure can be achieved by either hardware demodulation method or digital signal processing technique.

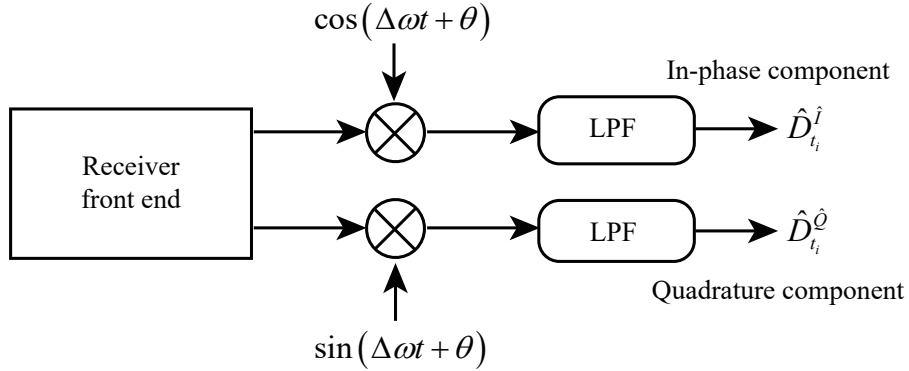


FIG. 6. Extraction of in-phase and quadrature components from measured results. LPF: low-pass filter

Finally, the in-phase result and the quadrature result can be deduced, given by

$$\begin{aligned} \hat{D}_{t_i}^I &= [\hat{D}_{t_i} \cos(\Delta\omega t + \theta)] * h_{LPF}(t) \\ &= S_0(t) * g(t)|_{t=t_i} \cdot \hat{I}_\xi, \end{aligned} \quad (91)$$

$$\begin{aligned} \hat{D}_{t_i}^Q &= [\hat{D}_{t_i} \sin(\Delta\omega t + \theta)] * h_{LPF}(t) \\ &= S_0(t) * g(t)|_{t=t_i} \cdot \hat{Q}_\xi. \end{aligned} \quad (92)$$

### Temporal mode matching

The measurement issue can be analyzed in a way that matches the experiment better, namely, the temporal mode matching scenarios.

In order to normalize the measured data, we need to divide the measured data by the standard deviation of shot noise  $\sigma_{\text{SNU}}(t_i) = \sqrt{V_0^{t_i}}$ . After sampling process (considering the detection transfer function) and SNU normalization, the result is given by

$$\begin{aligned}\hat{D}_{t_i}^{\text{SNU}} &= \frac{\hat{D}_{t_i}}{\sigma_{\text{SNU}}(t_i)} \\ &= \frac{1}{\sigma_{\text{SNU}}(t_i)} \int_{t_i}^{t_i+\Delta t_s} dt \int dt' \xi_{\text{LO},0}(t') \hat{X}_{\hat{a}}^{\omega_{\text{LO}}t'+\theta} g(t-t') \\ &= \frac{1}{\sigma_{\text{SNU}}(t_i)} \int dt' \xi_{\text{LO},0}(t') \hat{X}_{\hat{a}}^{\omega_{\text{LO}}t'+\theta} \int_{t_i}^{t_i+\Delta t_s} dt g(t-t').\end{aligned}\quad (93)$$

By defining the integrated detection function  $G^{t_i, \Delta t_s}(t') = \int_{t_i}^{t_i+\Delta t_s} dt g(t-t')$ , we can obtain the variance of shot noise at time  $t_i$ , which reads

$$\begin{aligned}\sigma_{\text{SNU}}^2(t_i) &= \langle 0 | \hat{D}_{t_i} \hat{D}_{t_i} | 0 \rangle \\ &= \left[ \int dt' \xi_{\text{LO},0}(t') G^{t_i, \Delta t_s}(t') \right]^2 \langle 0 | \left( \hat{X}_{\hat{a}}^{\omega_{\text{LO}}t'+\theta} \right)^2 | 0 \rangle \\ &= \left[ \int dt' \xi_{\text{LO},0}(t') G^{t_i, \Delta t_s}(t') \right]^2.\end{aligned}\quad (94)$$

Here  $\sigma_{\text{SNU}}(t) = \int dt' \xi_{\text{LO},0}(t') G^{t, \Delta t_s}(t')$  is defined as the standard deviation of the shot noise at time  $t$ . In the temporal mode description, we can see that SNU calibration is actually the process of calibrating measurement devices. All the spectrum-related information of detector and LO are involved.

Combing Eqs. (93,94), we can get

$$\begin{aligned}\hat{D}_{t_i}^{\text{SNU}} &= \frac{1}{\sigma_{\text{SNU}}(t_i)} \int dt' \xi_{\text{LO},0}(t') G^{t_i, \Delta t_s}(t') \hat{X}_{\hat{a}}^{\omega_{\text{LO}}t'+\theta}, \\ &= \int dt \frac{\xi_{\text{LO},0}(t) G^{t_i, \Delta t_s}(t)}{\sigma_{\text{SNU}}(t_i)} [\hat{a}(t) \exp[-i(\omega_{\text{LO}}t + \theta)] + \hat{a}^\dagger(t) \exp[i(\omega_{\text{LO}}t + \theta)]].\end{aligned}\quad (95)$$

By using Eq. (76), operator  $\hat{a}(t)$  can be mapped from frequency  $\omega_s$  to the baseband, namely,  $\hat{a}(t) = \hat{a}_0(t) \exp(i\omega_s t)$ , the calibrated result can be rewritten, given by

$$\hat{D}_{t_i}^{\text{SNU}} = \int dt \frac{\xi_{\text{LO},0}(t) G^{t_i, \Delta t_s}(t)}{\sigma_{\text{SNU}}(t_i)} [\hat{a}_0(t) \exp[-i(\Delta\omega t + \theta)] + \hat{a}_0^\dagger(t) \exp[i(\Delta\omega t + \theta)]].\quad (96)$$

We can then define an IF-related temporal mode  $\Xi_{\Delta\omega}^{t_i}(t)$ , given by

$$\Xi_{\Delta\omega}^{t_i}(t) = \frac{\xi_{\text{LO},0}(t) G^{t_i, \Delta t_s}(t)}{\sigma_{\text{SNU}}(t_i)} \exp(i\Delta\omega t),\quad (97)$$

and it is not difficult to prove that this mode meets the normalization condition  $\int dt |\Xi_{\Delta\omega}^{t_i}(t)|^2 = 1$ . This temporal mode represents the projection of the point  $t_i$  of the measured quantum state on the phase space rotating at speed  $\Delta\omega$ .

Using similar form as shown in Eq. (43), we can also define the field creation operator as

$$\hat{A}^\dagger(\Xi_{\Delta\omega}^{t_i}) = \int dt \Xi_{\Delta\omega}^{t_i}(t) \hat{a}_0^\dagger(t),\quad (98)$$

which can be treated as the projection of operator  $\hat{a}_0^\dagger(t)$  on basis  $\Xi_{\Delta\omega}^{t_i}(t)$ . The final result in Eq. (97) is then rewritten

as

$$\begin{aligned}\hat{D}_{t_i}^{\text{SNU}} &= \hat{A}^\dagger (\Xi_{\Delta\omega}^{t_i}) \exp(i\theta) + \hat{A} (\Xi_{\Delta\omega}^{t_i}) \exp(-i\theta) \\ &= \hat{X}_\theta (\Xi_{\Delta\omega}^{t_i}).\end{aligned}\quad (99)$$

Therefore, all the measurement results can be treated as the quadrature measurement of the temporal mode  $\Xi_{\Delta\omega}^{t_i}$ , which is composed of the parameters from both measurement side and the signal to be measured. Now considering a practical situation where the measured state is a wave-packet coherent state  $|\gamma\rangle$  given by Eq. (54), we can expand operator  $\hat{a}_0(t)$  as  $\hat{a}_0(t) = \xi_0(t) \hat{A}(\xi_0)$ , and Eq. (98) is rewritten as

$$\hat{A}^\dagger (\Xi_{\Delta\omega}^{t_i}) = \int dt \Xi_{\Delta\omega}^{t_i}(t) \xi_0(t) \hat{A}^\dagger (\xi_0), \quad (100)$$

where  $\int dt \Xi_{\Delta\omega}^{t_i}(t) \xi_0(t)$  quantifies the overlapping envelope (or basis) between measured signals and the measurement device, and it is also treated as the projection of the temporal mode  $\Xi_{\Delta\omega}^{t_i}(t)$  on the basis  $\xi_0(t)$ .

Using the Gram-Schmidt process, we can map the measured operator from the basis  $\Xi_{\Delta\omega}^{t_i}(t)$  to the set of bases  $\{\xi_0(t), \Psi_\perp(t)\}$ . In this transformation, the basis  $\Xi_{\Delta\omega}^{t_i}(t)$  represents the measurement mode-matched basis function;  $\xi_0(t)$  is the projection of the measurement basis onto the input states, and the orthogonal basis  $\Psi_\perp(t)$  is the projection of the measured results onto the non-mode-matched background. The Gram-Schmidt process is given as follows:

- Step 1: We can define the overlapping basis as

$$\sqrt{\eta_{\Delta\omega}^{t_i}} = \int dt \Xi_{\Delta\omega}^{t_i}(t) \xi_0(t). \quad (101)$$

- Step 2: The in-phase basis is written as  $\zeta_1(t) = \xi_0(t)$  directly.
- Step 3: The second orthonormal basis is calculated by

$$\begin{aligned}\zeta_2(t) &= \Xi_{\Delta\omega}^{t_i}(t) - \frac{\int dt \Xi_{\Delta\omega}^{t_i}(t) \zeta_1(t)}{\int dt \zeta_1^*(t) \zeta_1(t)} \zeta_1(t) \\ &= \Xi_{\Delta\omega}^{t_i}(t) - \sqrt{\eta_{\Delta\omega}^{t_i}} \xi_0(t).\end{aligned}\quad (102)$$

It is not hard to verify that

$$\begin{aligned}\int dt \zeta_2^*(t) \zeta_2(t) &= \int dt \left[ (\Xi_{\Delta\omega}^{t_i}(t))^* - \sqrt{\eta_{\Delta\omega}^{t_i}} \xi_0^*(t) \right] \left[ \Xi_{\Delta\omega}^{t_i}(t) - \sqrt{\eta_{\Delta\omega}^{t_i}} \xi_0(t) \right] \\ &= \int dt \left[ (\Xi_{\Delta\omega}^{t_i}(t))^* \Xi_{\Delta\omega}^{t_i}(t) + \eta_{\Delta\omega}^{t_i} \xi_0^*(t) \xi_0(t) - 2\sqrt{\eta_{\Delta\omega}^{t_i}} \xi_0^*(t) \Xi_{\Delta\omega}^{t_i}(t) \right] \\ &= 1 + \eta_{\Delta\omega}^{t_i} - 2\sqrt{\eta_{\Delta\omega}^{t_i}} \int dt \xi_0(t) \Xi_{\Delta\omega}^{t_i}(t) \\ &= 1 - \eta_{\Delta\omega}^{t_i}.\end{aligned}\quad (103)$$

After normalizing the basis function, we can obtain that

$$\begin{aligned}\Psi_\perp(t) &= \frac{\zeta_2(t)}{\sqrt{\int dt \zeta_2^*(t) \zeta_2(t)}} \\ &= \frac{1}{\sqrt{1 - \eta_{\Delta\omega}^{t_i}}} \left( \Xi_{\Delta\omega}^{t_i}(t) - \sqrt{\eta_{\Delta\omega}^{t_i}} \xi_0(t) \right).\end{aligned}\quad (104)$$

Now we can analyze the whole measurement process in by combing Eqs. (99,100,101). we can rewrite the measurement results by projecting the measurement operator onto the signal basis, given by

$$\hat{D}_{t_i}^{\text{SNU}} = \sqrt{\eta_{\Delta\omega}^{t_i}} \hat{X}_\theta(\xi_0) + \sqrt{1 - \eta_{\Delta\omega}^{t_i}} \hat{X}_\theta(\Psi_\perp), \quad (105)$$

and the projection of the background does not contribute to the measurement results. We can see that from Eq. (105), the practical measurement result is actually equivalent to the attenuation of the real modulation component, and its attenuation coefficient is the projection of the measurement operator on the input quantum state.

We know that the attenuation coefficient obeys the relation

$$\begin{aligned}\sqrt{\eta_{\Delta\omega}^{t_i}} &= \int dt \Xi_{\Delta\omega}^{t_i}(t) \xi_0(t) \\ &\leq \int dt \Xi_{\Delta\omega}^{t_i}(t) \Xi_{\Delta\omega}^{t_i}(t) \int dt \xi_0(t) \xi_0(t) \\ &= 1.\end{aligned}\tag{106}$$

For mode matching, which indicates that the actual measurement results are consistent with the real temporal mode of input states, we need to make the coefficient of the operator becomes 1. Assume the matched filter function is  $f_{\text{MF}}(x)$  and the output after processing is given by

$$\hat{D}_{t_i}^{\text{SNU}} = f_{\text{MF}}\left(\sqrt{\eta_{\Delta\omega}^{t_i}}\right) \hat{X}_\theta(\xi_0) + f_{\text{MF}}\left(\sqrt{1 - \eta_{\Delta\omega}^{t_i}}\right) \hat{X}_\theta(\Psi_\perp),\tag{107}$$

so we need to process the data so that  $f_{\text{MF}}\left(\sqrt{\eta_{\Delta\omega}^{t_i}}\right) = 1$ .

If the input state satisfies that  $\xi_0(t) = \Xi_{\Delta\omega}^{t_i}(t)$ , which means that the measured spectrum matches the received signal's spectrum, the measurement result is always true. Otherwise, we need to multiply a mode-matching factor at the receiving side to recover the signal.

This process is valid since the temporal mode description converts the calculation of  $q$ -number to the calculation of  $c$ -number.

## STATISTICS: FIRST- AND SECOND-ORDER MOMENTS

In CV-QKD, it is important to estimate the statistical information of the measured data, especially in the use of the extremality of Gaussian states [5]. In this section, we derive the first- and second-order moments of the measured results. Here, only single point sampling on one pulse is considered.

### Shot noise unite calibration

Shot noise unite (SNU) is an significant parameter for the normalization of measurement results in CV-QKD. Considering the scenario of vacuum state measurement, by using Eq. (90), the mean value of the measurement result at time  $t_i$  in each pulse is given by

$$\begin{aligned}d_0^{t_i} &= \langle 0 | \hat{D}_{t_i} | 0 \rangle \\ &= [S_0(t) * g(t)] \left[ \langle 0 | \hat{I}_\xi | 0 \rangle \cos(\Delta\omega t + \theta) - i \langle 0 | \hat{Q}_\xi | 0 \rangle \sin(\Delta\omega t + \theta) \right] \Big|_{t=t_i} \\ &= 0,\end{aligned}\tag{108}$$

where we ignore the fixed gain factor of the measured result, and using Eq. (89), the variance at sampling position  $t_i$  is given by

$$\begin{aligned}V_0^{t_i} &= \langle 0 | \left( \hat{D}_{t_i} \right)^2 | 0 \rangle \\ &= \langle 0 | \left( a \hat{A}^\dagger(\xi) + b \hat{A}(\xi) \right)^2 | 0 \rangle \\ &= \langle 0 | a^2 \hat{A}^\dagger(\xi) \hat{A}^\dagger(\xi) + b^2 \hat{A}(\xi) \hat{A}(\xi) + ab \left( \hat{A}^\dagger(\xi) \hat{A}(\xi) + \hat{A}(\xi) \hat{A}^\dagger(\xi) \right) | 0 \rangle \\ &= ab \\ &= \left( S_0(t) * g(t) \Big|_{t=t_i} \right)^2.\end{aligned}\tag{109}$$



where we use the notations

$$a = S_0(t) * g(t) \exp[i(\Delta\omega t + \theta)]|_{t=t_i}, \quad (110)$$

$$b = S_0(t) * g(t) \exp[-i(\Delta\omega t + \theta)]|_{t=t_i}, \quad (111)$$

and the relations of number states under continuous-mode representation [4], given by

$$\hat{A}(\xi_i)|n_i\rangle = \sqrt{n_i}|n_i - 1\rangle, \quad (112)$$

$$\hat{A}^\dagger(\xi_i)|n_i\rangle = \sqrt{n_i + 1}|n_i + 1\rangle, \quad (113)$$

$$\hat{A}(\xi_i)|0\rangle = 0. \quad (114)$$

We can see that from Eq. (109), the variance of shot noise is different from single-mode cases. Apart from the variance introduced by operator  $\hat{A}(\xi)$ , coefficient  $(S_0(t) * g(t)|_{t=t_i})^2$  is introduced into the measurement results. If the transmitted signal is flat or if the sampled point is the same as the point used for SNU calibration, the SNU calibration cannot influence the calculated results. Otherwise, we need to carefully consider the influence of SNU calibration. We also leave the optimization of SNU calibration for future study.

### First-order moment

Assume that Alice uses the IQ modulator to modulate both in-phase and quadrature components of the states with two sets of Gaussian random numbers  $\{x_A(t)\}$  and  $\{p_A(t)\}$ , each of which has zero mean value and variance  $V_A$ . We also assume the envelope of in-phase and quadrature components are the same. Therefore, the sampled photocurrent operator is then given by

$$\hat{D}_{t_i} = [S_0(t) * g(t)] \left[ x_A(t) \hat{I}_\xi \cos(\Delta\omega t + \theta) - ip_A(t) \hat{Q}_\xi \sin(\Delta\omega t + \theta) \right] \Big|_{t=t_i}. \quad (115)$$

For simplicity, here we only consider the in-phase component measurement as shown in Eq. (91), which is then written as

$$\hat{D}_{t_i}^{\hat{I}} = S_0(t) * g(t)|_{t=t_i} \cdot x(t_i) \hat{I}_\xi. \quad (116)$$

Under the measurement of wave-packet coherent states  $|\gamma\rangle$  as shown in Eq. (78), the mean value of the measurement result at time  $t_i$  in each pulse is given by

$$\begin{aligned} d_{\gamma}^{\hat{I}, t_i} &= \overline{\langle \gamma | \hat{D}_{t_i}^{\hat{I}} | \gamma \rangle} \\ &= S_0(t) * g(t)|_{t=t_i} \cdot \overline{x(t_i)} \langle \gamma | \hat{I}_\xi | \gamma \rangle \\ &= S_0(t) * g(t)|_{t=t_i} \cdot \overline{x(t_i)} \mathcal{R}(\gamma) \\ &= 0, \end{aligned} \quad (117)$$

where  $\overline{A}$  is the statistical average of  $A$  and  $\mathcal{R}$  denote the real part.

We can see that in the Gaussian modulation scenario, the first-order moment is still unchanged compared with the single-mode case. If the modulation method is not the Gaussian modulation, the statistical average value can be calculated in the similar way. We can also obtain the mean value of the quadrature component, namely,  $d_{\gamma}^{\hat{Q}, t_i} = 0$ .

### Second-order moment

The variance of the in-phase component can be obtained, which reads

$$\begin{aligned} V_{\gamma}^{\hat{I}, t_i} &= \overline{\langle \gamma | (\hat{D}_{t_i}^{\hat{I}})^2 | \gamma \rangle} \\ &= (S_0(t) * g(t)|_{t=t_i})^2 \overline{x^2(t_i)} \langle \gamma | \hat{I}_\xi^2 | \gamma \rangle \\ &= (S_0(t) * g(t)|_{t=t_i})^2 V_A. \end{aligned} \quad (118)$$

It is very interesting to find that the measured quadrature at fixed time  $t_i$  still satisfies a Gaussian distribution; therefore, the extremality of Gaussian states still holds. If the sampling point used for SNU calibration is the same as the sampling point used to generate secret keys, the normalized variance is given by

$$V_{\gamma, \text{norm}}^{\hat{I}, t_i} = \frac{V_{\gamma}^{\hat{I}, t_i}}{V_0^{t_i}} = V_A, \quad (119)$$

which is exactly the same as the single-mode cases.

However, if the sampling point used for SNU calibration is not the same as the sampling point used to generate secret keys, we must use the envelope-related information to estimate the modified variance, which is given by

$$V_{\gamma, t_j}^{\hat{I}, t_i} = \frac{V_{\gamma}^{\hat{I}, t_j}}{V_0^{t_i}} = \left( \frac{S_0(t) * g(t)|_{t=t_j}}{S_0(t) * g(t)|_{t=t_i}} \right)^2 V_A \quad (120)$$

$$= \eta(t_i, t_j) V_A, \quad (121)$$

where the envelope-related factor is written by

$$\eta(t_i, t_j) = \left( \frac{S_0(t) * g(t)|_{t=t_j}}{S_0(t) * g(t)|_{t=t_i}} \right)^2. \quad (122)$$

Under this model, the timing jitter, the channel dispersion and other envelope distortion issues can be solved by comparing the positions of measuring points on the envelope before and after calibration.

## TRANSMISSION MODEL

In this section, generalized channel model in CV-QKD, namely, the continuous-mode channel is considered, and the quadrature description is given.

### Continuous-mode channel considerations

Under the transmission of continuous-mode fields, since single-mode Gaussian operations are insufficient for describing the whole features of channels, continuous-mode Gaussian operators need to be used to address this issue.

In continuous-mode cases, the transmission of a quantum state can be modeled by a frequency-dependent BS, and  $\tau(\omega)$  is the transmission coefficient of the channel. Assuming that the operator of the input signal is described by  $\hat{a}_{\text{in}}(\omega)$ , the model of a frequency-dependent BS can be written as [7]

$$\mathbf{S}_{\text{BS}}(\omega) = \begin{pmatrix} \sqrt{\tau(\omega)} & \sqrt{1-\tau(\omega)} \\ -\sqrt{1-\tau(\omega)} & \sqrt{\tau(\omega)} \end{pmatrix}, \quad (123)$$

and the input-output relation of the signal through the BS is given by

$$\begin{pmatrix} \hat{a}_{\text{out}}(\omega) \\ \hat{b}_{\text{out}}(\omega) \end{pmatrix} = \mathbf{S}_{\text{BS}}(\omega) \begin{pmatrix} \hat{a}_{\text{in}}(\omega) \\ \hat{b}(\omega) \end{pmatrix}, \quad (124)$$

where  $\hat{b}(\omega)$  is an annihilation operator (or a heat bath) introduced by the environment. It can be proven that the continuous-mode BS model still satisfies the boson commutation relation, which reads

$$[\hat{a}_{\text{out}}(\omega), \hat{a}_{\text{out}}^\dagger(\omega')] = \delta(\omega - \omega'). \quad (125)$$

Considering a general quantum channel in CV-QKD, the model can be given as shown in Fig. 7.

In this scenario, suppose that there are  $N$  cascaded BSs, which are arranged at equal intervals. Assuming that the total transmission distance is  $z$  and that the spacing of each BS is  $\Delta z$ , the following relation holds:

$$N = z/\Delta z. \quad (126)$$

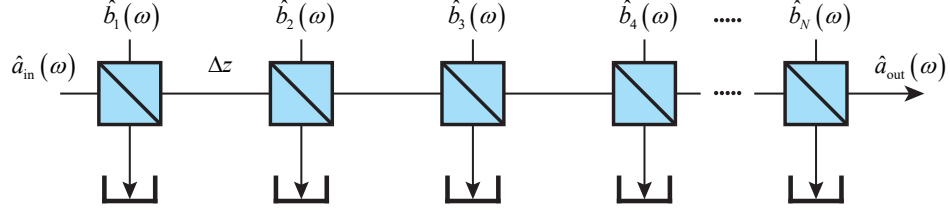


FIG. 7. A general channel transmission model.

Here, it is assumed that there is a small phase shift for each distance  $z$ , which is given by  $\exp(ik_r(\omega)\Delta z)$ . After each BS, two effects are imposed on the signal. One is the attenuation, and the other is the extra added phase shift. The former is modeled by the BS, and the latter is considered to be caused by a small delay. The wave vector  $k(\omega)$  then has the following dispersion relation:

$$k(\omega) = k_r(\omega) + ik_i(\omega), \quad (127)$$

where the real part denotes the phase shift caused by the delay, and the imaginary part represents the attenuation introduced by the BS. After passing the  $N$  cascaded BSs, the output

$$\begin{aligned} \hat{a}_{\text{out}}(\omega) &= \left[ \sqrt{\tau(\omega)} \exp(ik_r\Delta z) \right]^N \hat{a}_{\text{in}}(\omega) \\ &+ \sqrt{1-\tau(\omega)} \sum_{m=1}^N \left[ \sqrt{\tau(\omega)} \exp(ik_r\Delta z) \right]^{N-m} \hat{b}_m(\omega), \end{aligned} \quad (128)$$

and all the environment operators are assumed to be independent, satisfying the following boson commutation relation:

$$[\hat{b}_m(\omega), \hat{b}_n^\dagger(\omega')] = \delta_{mn} \delta(\omega - \omega'). \quad (129)$$

The real part of the wave vector is defined by

$$k_r(\omega) = \omega n(\omega)/c, \quad (130)$$

and the imaginary part of the wave vector is defined by

$$k_i(\omega) = [1 - \tau(\omega)]/2\Delta z, \quad (131)$$

so we can obtain

$$\tau^N(\omega) = [1 - 2k_i(\omega)\Delta z]^N = [1 - 2k_i(\omega)z/N]^N. \quad (132)$$

When the number of BSs tends to infinity,

$$N \rightarrow \infty, \Delta z \rightarrow 0, \tau(\omega) \rightarrow 1, \quad (133)$$

we can obtain

$$\tau^N(\omega) \rightarrow \exp(-2k_i(\omega)z). \quad (134)$$

In continuous-mode cases, the environment operator can also be written in continuous-mode form, which is given by

$$\hat{b}_m(\omega) \rightarrow (\Delta z)^{1/2} \hat{b}(\omega, z'), \quad (135)$$

$$\delta_{mn} \rightarrow \Delta z \delta(z' - z''), \quad (136)$$

and the continuous-mode commutation relation satisfies the boson commutator, which reads as follows:

$$\left[ \hat{b}(\omega, z), \hat{b}^\dagger(\omega', z') \right] = \delta(\omega - \omega') \delta(z - z'). \quad (137)$$

After converting discrete sums to continuous integrals, the continuous-mode operator output after the quantum channels can be rewritten as

$$\begin{aligned} \hat{a}_{\text{out}}(\omega) &= \exp[-k_i(\omega)z] \exp[ik_r(\omega)z] \hat{a}_{\text{in}}(\omega) \\ &+ \sqrt{2k_i(\omega)} \int_0^z dz' \exp\{[ik_r(\omega) - k_i(\omega)](z - z')\} \hat{b}(\omega, z'). \end{aligned} \quad (138)$$

From Eq. (138), it can be seen that different from single-mode cases, the security analysis changes when the continuous mode is considered. In a general transmission medium with frequency-dependent attenuation and dispersion, there are generally two effects that influence the transmitted signals in the first term of Eq. (138). The first is the attenuation coefficient  $\exp[-k_i(\omega)z]$  introduced through the channel, and the second is the additional phase shift induced by dispersion  $\exp[ik_r(\omega)z]$ , especially in dispersion media.

The first effect is similar to that of the single-mode case considered in the original CV-QKD protocols. The only difference is that it has different attenuations for different signal frequencies. However, when the linewidth is narrow compared to the central frequency, the attenuation can be approximately considered to be independent of the frequencies.

The second effect is the dispersion caused by continuous-mode signals traveling through the dispersive media, which cannot be ignored. In particular, the pulse transmission rate is considerable, especially in dispersive media such as optical fibers, and directly affects the security analysis of the whole protocol. Due to the different times required to reach the detector at different frequencies in the dispersive medium, the shape of the measured signal will change. To satisfy the measurable parameters in practical experiments, we rewrite the real part of the wave vector by exploiting Taylor expansion, which is a common method in classical optical communication. Then, we obtain

$$k_r(\omega) = k_0 + k_1(\omega - \omega_0) + \frac{1}{2!}k_2(\omega - \omega_0)^2 + \dots, \quad (139)$$

where

$$k_0 = \frac{\omega_0 n(\omega_0)}{c}, \quad (140)$$

$$k_1 = \left. \frac{\partial k_r(\omega)}{\partial \omega} \right|_{\omega=\omega_0} = \frac{1}{v_G}, \quad (141)$$

$$k_2 = \left. \frac{\partial^2 k_r(\omega)}{\partial \omega^2} \right|_{\omega=\omega_0}, \quad (142)$$

where  $k_0$  denotes the normal phase shift,  $k_1$  denotes the inverse group velocity, and  $k_2$  is the second-order dispersion coefficient.

To facilitate the follow-up analysis, we divide Eq. (138) into two parts. The first term  $\hat{a}_{\text{out},1}(\omega)$  considers the evolution of the transmitted signals through the channel, and the second term  $\hat{a}_{\text{out},2}(\omega)$  considers the influence of the environment.

The first term of Eq. (138) can be further transformed to obtain the signal transmitted in the time domain. Assuming that the linewidth is small enough compared to the central frequency of the signal, the relation  $k_i(\omega) \approx k_i$  holds, and the Fourier frequency is chosen as  $\Omega = \omega - \omega_0$ . Then, we can obtain

$$\begin{aligned} \hat{a}_{\text{out},1}(t, z) &= \frac{1}{2\pi} \int d\Omega \hat{a}_{\text{in}}(\Omega) \exp(-k_i z) \cdot \exp \left[ i \left( k_0 + k_1 \Omega + \frac{k_2}{2} \Omega^2 \right) z \right] \exp(-i\Omega t) \\ &= \varphi(z) \mathcal{F}^{-1} [\hat{a}_{\text{in}}(\Omega) H(\Omega, z)], \end{aligned} \quad (143)$$



where  $\mathcal{F}^{-1}(\cdot)$  denotes the inverse Fourier transfer, and

$$\varphi(z) = \exp(ik_0 z), \quad (144)$$

$$\hat{a}_{\text{in}}(\Omega) = \hat{a}_{\text{in}}(\omega_0 + \Omega), \quad (145)$$

$$H(\Omega, z) = \exp\left(-k_i z + ik_1 \Omega z + i\frac{k_2}{2} \Omega^2 z\right), \quad (146)$$

where  $\varphi(z)$  denotes a determined phase shift and  $H(\Omega, z)$  represents the frequency-dependent transfer function of the channel. From the result of Eq. (143), two effects are introduced while quantum signals propagate through the channel, namely, an additional fixed phase shift  $\exp(ik_0 z)$  and a transfer function caused by the attenuation and dispersion introduced by the channel.

If the transmitted medium is colorless, such as in free space transmission where  $k_2 = 0$ , the pulses only have  $k_1 z$  delays without changing their shapes. However, if the pulses are transmitted over a dispersive medium, such as fiber, this scenario leads to pulse distortion.

The second term of Eq. (138) denotes the noise introduced by the environment. In the case of the narrow linewidth approximation, this term can be rewritten as

$$\hat{a}_{\text{out},2}(\omega) \approx \sqrt{2k_i} \int_0^z dz' \exp\{[ik_r(\omega) - k_i](z - z')\} \hat{b}(\omega, z'). \quad (147)$$

To further simplify the analysis, we use the ensemble average through the transmission direction to replace the operator  $\hat{b}(\omega, z)$ , as shown in Fig. 8; thus, the operators introduced by the environment are supposed to be independent of the distances, which means that

$$\hat{b}(\omega, z') \rightarrow \langle \hat{b}(\omega, z) \rangle_z = \hat{b}(\omega). \quad (148)$$

This assumption is reasonable in most experiments since we can always find the total noise at the receiver side. However, we also note that the ensemble average may not consider the most general attack, and we leave this issue for further investigation.

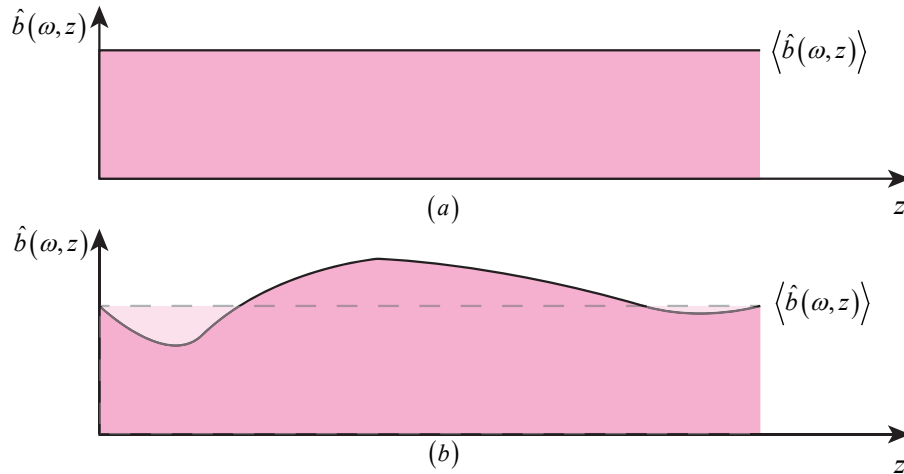


FIG. 8. An environment operator through the channel. (a) shows environment noise that does not vary with time, and (b) shows environment noise that varies with time.

Therefore, it can be obtained that the term introduced by the environment is approximately described by

$$\begin{aligned} \hat{a}_{\text{out},2}(\omega) &= \sqrt{1 - \tau^2(\omega)} \hat{b}(\omega) \\ &= \sqrt{1 - \exp(-2k_i z)} \hat{b}(\omega). \end{aligned} \quad (149)$$

Consequently, the simplified form of Eq. (138) becomes

$$\begin{aligned}\hat{a}_{\text{out}}(\omega, z) &= \exp(-k_i z) \exp[ik_r(\omega)z] \hat{a}_{\text{in}}(\omega) + \sqrt{1 - \exp(-2k_i z)} \hat{b}(\omega) \\ &= \sqrt{\tau} \exp[ik_r(\omega)z] \hat{a}_{\text{in}}(\omega) + \sqrt{1 - \tau} \hat{b}(\omega),\end{aligned}$$

and by combining Eq. (143) and Eq. (149), the corresponding outcome in the time domain has the following form:

$$\hat{a}_{\text{out}}(t, z) = \varphi(z) \mathcal{F}^{-1}[\hat{a}_{\text{in}}(\Omega) H(\Omega, z)] + \sqrt{1 - \exp(-2k_i z)} \hat{b}(t). \quad (150)$$

Thus, the overall outcomes after the quantum channels are given by

$$\begin{pmatrix} \hat{a}_{\text{out}}(\omega, z) \\ \hat{b}_{\text{out}}(\omega, z) \end{pmatrix} = \mathbf{M} \begin{pmatrix} \hat{a}_{\text{in}}(\Omega) \\ \hat{b}(\omega) \end{pmatrix}, \quad (151)$$

where

$$\mathbf{M} = \begin{pmatrix} \frac{H(\Omega, z)}{-\sqrt{1 - H^2(\Omega, z)}} & \sqrt{1 - H^2(\Omega, z)} \\ \sqrt{1 - H^2(\Omega, z)} & H(\Omega, z) \end{pmatrix} \quad (152)$$

is the transfer function of the frequency-dependent channel matrix.

The final output modes obtained after passing through the quantum channel can be further simplified and rewritten as

$$\hat{a}_{\text{out}}(t, z) = \hat{a}_{\text{in}}(t) * h(t, z) + \hat{n}(t), \quad (153)$$

where  $h(t, z)$  is the channel transfer function in the time domain and  $\hat{n}(t)$  denotes the introduced channel noise given by  $\hat{n}(t) = \sqrt{1 - \tau} \hat{b}(t)$ .

We note that Eq. (153) is very similar to the classical communication scenarios; therefore, numerous techniques can be exploited to analyze the transmission issues in quantum cryptography.

Moreover, considering the pulse propagation cases, it can be proven that the channel transfer function only acts on the wave packet function of the transmitted operator, which is a  $c$ -number transformation, resulting in a simplified subsequent analysis.

Utilizing the non-continuous basis formula shown in Eq. (44) again, Eq. (153) can be rewritten in the following form:

$$\hat{a}_{\text{out}}(t, z) = [\xi(t) * h(t, z)] \hat{A}(\xi) + \sqrt{1 - \tau} \hat{b}(t), \quad (154)$$

and the pulse propagation in a quantum channel scenario can be obtained.

It should be noted that in practical cases, the assumption that the environment operator  $\hat{b}(t, z)$  is independent of the transmission distance does not hold, since the variation of each channel segment may not be uniform (especially for long links), and the analysis of the environment becomes more involved. We leave this issue for further investigation.

### Measurement results via quadrature descriptions

By using Eqs. (60, 154), we can obtain the measurement result after transmission through the quantum channel, which is given by

$$\begin{aligned}\hat{O}(t) &= \int_t^{t+T} dt \left( \hat{a}_{\text{out}}^\dagger(t) a_{\text{LO}}(t) + \hat{a}_{\text{LO}}^\dagger(t) a_{\text{out}}(t) \right) \\ &= \int_t^{t+T} dt \left[ \left( \xi_{\text{out}}(t) \hat{A}(\xi) + \sqrt{1 - \tau} \hat{b}(t) \right)^\dagger \xi_{\text{LO}}(t) \hat{A}_{\text{LO}}(\xi) \right] \\ &\quad + \int_t^{t+T} dt \left[ \xi_{\text{LO}}^*(t) \hat{A}_{\text{LO}}^\dagger(\xi) \left( \xi_{\text{out}}(t) \hat{A}(\xi) + \sqrt{1 - \tau} \hat{b}(t) \right) \right].\end{aligned} \quad (155)$$

We also give the following notations for further simplifying this result:  $\xi_{\text{out}}(t) = \xi_{\text{out},0}(t) \exp(i(\omega_s t + \theta_{\text{out}}))$ ,  $\hat{b}(t) = \hat{b}_0 \exp(i\omega_s t)$ , where  $\theta_{\text{out}}$  is the relative phase of signals after transmission, and  $\xi_{\text{out},0}(t)$  and  $\hat{b}_0$  are the baseband

transfer functions of output signal and quantum noise, respectively.

Assuming the detection integration time is small compared to the signal variation time, we can then deduce the measurement result as

$$\begin{aligned} \hat{O}(t) = & T_{\xi_{\text{LO}}}(t) \xi_{\text{out},0}(t) \left[ \hat{A}^\dagger(\xi) \hat{A}_{\text{LO}}(\xi) \exp(-i(\Delta\omega t + \theta_{\text{out}})) + \hat{A}_{\text{LO}}^\dagger(\xi) \hat{A}(\xi) \exp(i(\Delta\omega t + \theta_{\text{out}})) \right] \\ & + T_{\xi_{\text{LO}}}(t) \sqrt{1-\tau} \left[ \hat{b}_0^\dagger \hat{A}_{\text{LO}}(\xi) \exp(-i\Delta\omega t) + \hat{A}_{\text{LO}}^\dagger(\xi) \hat{b}_0 \exp(i\Delta\omega t) \right]. \end{aligned} \quad (156)$$

After averaging the LO's effect, the photocurrent operator can be then written as

$$\begin{aligned} \hat{O}_s(t) = & {}_{\text{LO}} \langle \mu | \hat{O}(t) | \mu \rangle_{\text{LO}} \\ = & T \mu_{\text{LO}}^{1/2} \xi_{\text{LO},0}(t) \xi_{\text{out},0}(t) \left[ \hat{A}^\dagger(\xi) \exp(-i(\Delta\omega t + \theta_{\text{out}})) + \hat{A}(\xi) \exp(i(\Delta\omega t + \theta_{\text{out}})) \right] \\ & + T \mu_{\text{LO}}^{1/2} \xi_{\text{LO}}(t) \sqrt{1-\tau} \left[ \hat{b}_0^\dagger \exp(-i\Delta\omega t) + \hat{b}_0 \exp(i\Delta\omega t) \right] \\ = & T \mu_{\text{LO}}^{1/2} \xi_{\text{LO}}(t) \left[ \xi_{\text{out},0}(t) \hat{X}_\xi^{\Delta\omega t + \theta_{\text{out}}} + \sqrt{1-\tau} \hat{X}_{\hat{b}_0}^{\Delta\omega t} \right], \end{aligned} \quad (157)$$

where  $\xi_{\text{out},0}(t) = \xi_0(t) * h(t, z)$  is the envelope after transmission ignoring the phase information, since all the phase information are considered in the quadrature operator, and  $\hat{X}_{\hat{b}_0}^{\Delta\omega t} = \hat{b}_0^\dagger \exp(-i\Delta\omega t) + \hat{b}_0 \exp(i\Delta\omega t)$  denotes the quadrature operator of the channel noise. After passing through the channel, the quadrature measurement is distorted by the transmitted pulses, and additional noise is added.

From the perspective of the frequency domain, since each output mode in continuous-mode states is exactly the same as that in the single-mode case, the modes are independent of each other due to the boson commutation relations; thus, the whole transmitted quantum state still satisfies the optimality of the Gaussian attack. We still need to construct the covariance matrix (CM) to calculate the security key rate.

The phase compensation technique can be used to eliminate the phase drift  $\theta_{\text{out}}$  compared to the initial phase  $\theta$ . With the use of appropriate phase compensation technologies, the pulse quadrature shown in Eq. (157) does not vary with the propagation process; thus, all of the influences on the signal quadratures lead to influences on the pulse shape, converting this issue to a  $c$ -number calculation.

The use of this method to express continuous-mode operators with non-continuous basis functions brings great convenience to the analysis of experimental results. In the subsequent analysis, we only need to consider the change in the pulse shape propagated in the medium, and the secret key rate can be obtained. Fortunately, the analysis of pulse propagation in media is a very mature topic in classical optical communication.

## ENTANGLEMENT-BASED MODEL

Entanglement-based (EB) schemes are crucial for theoretical analysis, and a proper virtual entanglement state is the key to constructing security proofs. Here we present the entanglement-based scheme of the proposed protocol.

### Continuous-mode two-photon coherent state

Considering the two-photon process in nonlinear cases, a continuous-mode two-photon coherent state (CTCS) in the time domain can be generated; this state has similar properties to those of the two-continuous-mode squeezed vacuum state (TCMSV). Here, we use the CTCS instead of the TCMSV to perform the EB analysis.

The two-photon wave package function is defined by the Fourier transform of the two-photon spectrum:

$$\beta(t, t') = \frac{1}{2\pi} \int d\omega \int d\omega' \beta(\omega, \omega') \exp(-i\omega t - i\omega' t'), \quad (158)$$

and the two-photon wave package function satisfies the normalized relation, which is given by

$$\int dt \int dt' |\beta(t, t')|^2 = 1. \quad (159)$$

Therefore, the photon pair creation operator in the time domain can be described by

$$\hat{P}_{ab}^\dagger(\beta) = \frac{1}{\sqrt{2}} \int dt \int dt' \beta(t, t') \hat{a}^\dagger(t) \hat{b}^\dagger(t'). \quad (160)$$

By defining the two-continuous-mode squeezed operator as

$$\hat{S}_2(\beta) = \exp\left(\hat{P}_{ab}(\beta) - \hat{P}_{ab}^\dagger(\beta)\right), \quad (161)$$

the CTCS is written as

$$|\text{CTCS}\rangle = \hat{S}_2(\xi) |00\rangle. \quad (162)$$

To address the issues of pulsed CTCSs, a complete set of non-continuous basis functions can also be used. Similar to Eq. (43), a two-mode wave packet creation operator  $\hat{A}^\dagger(\xi_i) \hat{B}^\dagger(\xi_i)$  can be obtained, which reads as follows:

$$\hat{A}^\dagger(\xi_i) \hat{B}^\dagger(\xi_i) = \int dt \int dt' \xi_i(t, t') \hat{a}^\dagger(t) \hat{b}^\dagger(t'), \quad (163)$$

and the operators  $\hat{a}(t) \hat{b}(t')$  can also be written as a superposition of the non-continuous field creation operators:

$$\hat{a}^\dagger(t) \hat{b}^\dagger(t') = \sum_i \xi_i^*(t, t') \hat{A}^\dagger(\xi_i) \hat{B}^\dagger(\xi_i), \quad (164)$$

and

$$\hat{S}_2(\beta) = \exp\left(\sum_i \Gamma_i^* \hat{A}(\xi_i) \hat{B}(\xi_i) - \Gamma_i \hat{A}^\dagger(\xi_i) \hat{B}^\dagger(\xi_i)\right), \quad (165)$$

where

$$\Gamma_i = \int dt \int dt' \beta(t, t') \xi_i^*(t, t'). \quad (166)$$

Therefore, the CTCS represented by the non-continuous basis function is rewritten as

$$\begin{aligned} |\text{CTCS}\rangle &= |\{\beta(t, t')\}\rangle = \hat{S}_2(\beta) |00\rangle \\ &= \prod_i |\Gamma_i\rangle = |\{\Gamma_i\}\rangle. \end{aligned} \quad (167)$$

The two states are symmetrically distributed, and the wave packet shapes of two modes are the same.

It should be noted that since each sampling step occurs at a specific position of the pulse and the CM is statistically obtained by measuring the samples of the ensemble many times, time  $t$  is only the sampling position in the marked pulse, which is equivalent to a coordinate in the pulse. This is completely different from the single-mode case, which does not need to consider the influence of the pulse sampling position on the measurement results.

If both Alice and Bob are sampled at the same pulse time, the whole CM is consistent with the traditional single-mode case, which is written as:

$$\mathbf{V}_{\text{TMSV}} = \begin{pmatrix} V\mathbf{I} & \sqrt{V^2 - 1}\mathbf{Z} \\ \sqrt{V^2 - 1}\mathbf{Z} & V\mathbf{I} \end{pmatrix}, \quad (168)$$

To consider a more general case, that is, the scenario in which the sampling positions of the pulses measured by Alice and Bob are different, the CTCS is expanded by using a discrete basis, and the following CM can be obtained:

$$\begin{aligned} \mathbf{V}_{\text{CTCS}}(t, t') &= \begin{pmatrix} \cosh 2\xi(t, t') \mathbf{I} & \sinh 2\xi(t, t') \mathbf{Z} \\ \sinh 2\xi(t, t') \mathbf{Z} & \cosh 2\xi(t, t') \mathbf{I} \end{pmatrix} \\ &= \begin{pmatrix} V_\xi(t, t') \mathbf{I} & \sqrt{V_\xi^2(t, t') - 1} \mathbf{Z} \\ \sqrt{V_\xi^2(t, t') - 1} \mathbf{Z} & V_\xi(t, t') \mathbf{I} \end{pmatrix}, \end{aligned} \quad (169)$$

where the wave package  $\xi(t, t')$  is not normalized. Here we use the following relations to perform the derivation:

$$\hat{S}_2^\dagger(\beta) \hat{a}(t) \hat{S}_2(\{\beta\}) = \hat{a}(t) \cosh[\xi(t, t')] - \hat{b}^\dagger(t') \sinh[\xi(t, t')], \quad (170)$$

$$\hat{S}_2^\dagger(\beta) \hat{b}(t') \hat{S}_2(\{\beta\}) = \hat{b}(t') \cosh[\xi(t, t')] - \hat{a}^\dagger(t) \sinh[\xi(t, t')]. \quad (171)$$

### Entanglement-based equivalence

Therefore, for the EB model, Alice always measures at the peak point of a pulse (which means that the relation  $t = t_0$  always holds), which corresponds to the ideal modulation in PM schemes, as shown in Fig. 9.

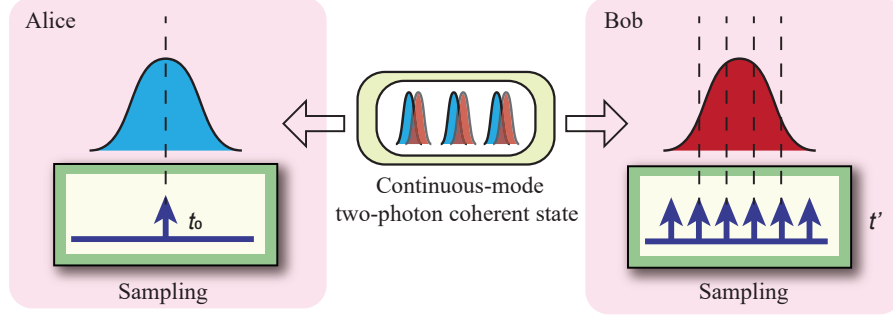


FIG. 9. Model of a continuous-mode two-photon coherent state (CTCS) and the entanglement-based scheme.

Since the form shown in Eq. (169) is the same as that in Eq. (168), which means that it has the same security as the single-mode case for a certain sampling point in the continuous-mode case, the EB scheme still holds by finding the modified variance of the CTCS.

If the sampling position of Bob is not the peak point of the pulse, the correlation between Alice's and Bob's measurement results is reduced. To maximize the correlation between Alice's and Bob's data, Alice needs to rescale her data to match the sampling-point on Bob's side. The CM after Bob's measurements and Alice's re-scaling becomes:

$$\mathbf{V}_{\text{CTCS}} = \begin{pmatrix} V_{\text{res}} \mathbf{I} & \sqrt{V_{\text{res}}^2 - 1} \mathbf{Z} \\ \sqrt{V_{\text{res}}^2 - 1} \mathbf{Z} & V_{\text{res}} \mathbf{I} \end{pmatrix}, \quad (172)$$

where  $V_{\text{res}} = \eta(t_0, t_j) V_A$  is the rescaled variance after calibrating the sampling point by using the relation shown in Eq. (121), and  $\eta(t_0, t_j)$  quantifies the correlation between the sampling point at the peak value ( $t = t_0$ ) and the sampling point at the time of  $t_j$ , which can be obtained by comparing the difference between the sampling point and the peak point. Similar form of the rescaled factor as Eq. (122) can be obtained, which reads

$$\eta(t_0, t_j) = \left( \frac{\xi_{\text{LO}}(t) \xi_0(t) * h(t) * g(t)|_{t=t_j}}{\xi_{\text{LO}}(t) \xi_0(t) * g(t)|_{t=t_0}} \right)^2. \quad (173)$$

To reduce the influence of LO's envelope on the measurement results, we usually select the LO as the optical signal with flat envelope, and therefore we have  $\xi_{\text{LO}}(t) = 1$ . Thus the simplified re-scaled factor is rewritten as

$$\eta(t_0, t_j) = \left( \frac{\xi_0(t) * h(t) * g(t)|_{t=t_j}}{\xi_0(t) * g(t)|_{t=t_0}} \right)^2. \quad (174)$$

The overall CM after passing through the channel is

$$\mathbf{V}_{\text{ab}}(t_0, t_j) = \begin{pmatrix} V_{\text{res}} \mathbf{I} & \sqrt{\tau} \sqrt{V_{\text{res}}^2 - 1} \mathbf{Z} \\ \sqrt{\tau} \sqrt{V_{\text{res}}^2 - 1} \mathbf{Z} & [\tau V_{\text{res}} + (1 - \tau) V_b] \mathbf{I} \end{pmatrix}, \quad (175)$$

where  $V_b$  is the noise variance introduced by the channel. The timing jitter introduced in synchronization processes, the sampling position on the pulse, and other time-domain-related issues can all be solved by rescaling the variance

of measured points.

We can see that in traditional single-mode CV-QKD, when  $t' \neq t_0$  and the rescaled operation is not performed, the unphysical regime may occur since different points on the pulse do not necessarily satisfy the uncertain relation, and these results cannot be handled in single-mode cases since they are actually derived from different measured states. However, this situation can be dealt with since one continuous mode is considered with different sampling points, and their correlations come from the shape of the state.

Utilizing the conclusion of traditional QKD, the variance introduced by Eve is given by

$$V_b = \left( \frac{\tau\varepsilon}{1-\tau} \right) + 1, \quad (176)$$

and the overall security analysis can be performed. We also leave the general attack's model for further investigations.

- 
- [1] R. Loudon, *The Quantum Theory of Light: 3rd Edition* (Oxford University Press, New York, 2000).
  - [2] C. M. Caves and B. L. Schumaker, New Formalism for Two-Photon Quantum Optics. I. Quadrature Phases and Squeezed States, *Phys. Rev. A* **31**, 3068 (1985).
  - [3] K. J. Blow, R. Loudon, S. J. D. Phoenix, T. J. Shepherd, Continuum fields in quantum optics, *Phys. Rev. A* **42**, 4102 (1990).
  - [4] D. J. Santos, R. Loudon, and F. J. Fraile-Peláez, Continuum States and Fields in Quantum Optics, *Am. J. Phys.* **65**, 126 (1997).
  - [5] M. M. Wolf, G. Giedke, and J. Ignacio Cirac, Extremality of Gaussian Quantum States, *Phys. Rev. Lett.* **96**, 080502 (2006).
  - [6] S. Kumar and M. J. Deen, *Fiber Optic Communications: Fundamentals and Applications* (Wiley, United Kingdom, 2014).
  - [7] J. R. Jeffers, N. Imoto, and R. Loudon, Quantum Optics of Traveling-Wave Attenuators and Amplifiers, *Phys. Rev. A* **47**, 3346 (1993).
-